AD-A179 773 SEMICONDUCTOR EUTECTIC SOLAR CELL(U) CALIFORNIA UNIV 1/2
LOS ANGELES SCHOOL OF ENGINEERING AND APPLIED SCIENCE
A S YUE ET AL. DEC 86 UCLA-ENG-8808 RADC-TR-86-170
UNCLASSIFIED F19628-77-C-0021 F/G 20/12 NL

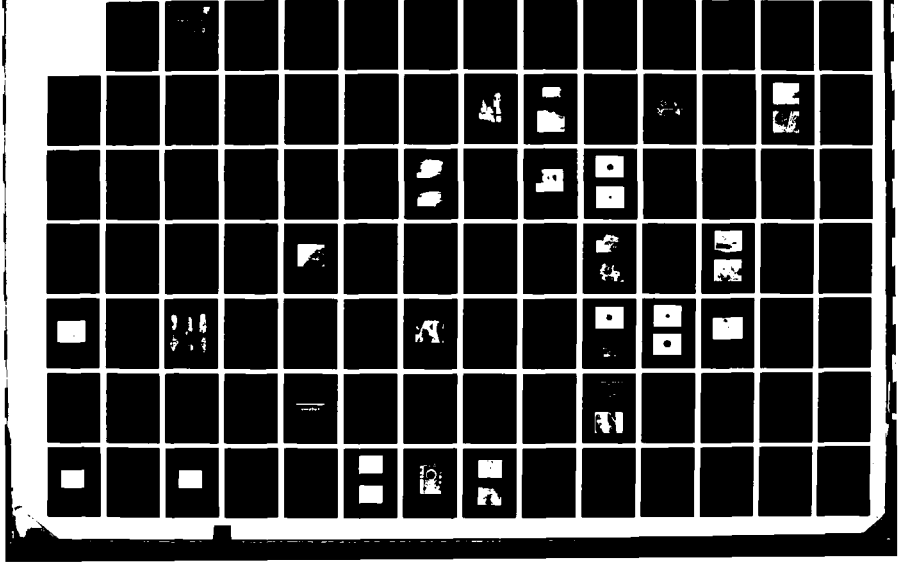

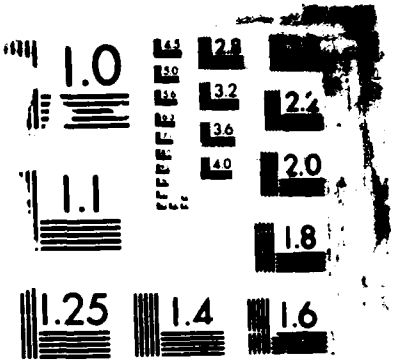
1.0
1.1
1.25
1.4
1.6
2.8
3.2
3.6
4.0
2.2
2.0
1.8

(12)

RADC-TR-86-170
Final Technical Report
December 1986

SEMICONDUCTOR EUTECTIC SOLAR CELL

University of California

A. S. Yue and J. G. Yu

ROME AIR DEVELOPMENT CENTER
Air Force Systems Command
Griffiss Air Force Base, NY 13441-5700

REPORT DOCUMENTATION PAGE

1a. REPORT SECURITY CLASSIFICATION UNCLASSIFIED	1b. RESTRICTIVE MARKINGS N/A
2a. SECURITY CLASSIFICATION AUTHORITY N/A	3. DISTRIBUTION/AVAILABILITY OF REPORT Approved for public release; distribution unlimited.
2b. DECLASSIFICATION/DOWNGRADING SCHEDULE N/A	
4. PERFORMING ORGANIZATION REPORT NUMBER(S) UCLA-ENG-8008	5. MONITORING ORGANIZATION REPORT NUMBER(S) RADC-TR-86-170
6a. NAME OF PERFORMING ORGANIZATION University of California 6b. OFFICE SYMBOL (If applicable)	7a. NAME OF MONITORING ORGANIZATION Rome Air Development Center (ESM)
6c. ADDRESS (City, State, and ZIP Code) School of Engineering & Applied Science Los Angeles CA 90024	7b. ADDRESS (City, State, and ZIP Code) Hanscom AFB MA 01731-5000
8a. NAME OF FUNDING/SPONSORING ORGANIZATION Rome Air Development Center 8b. OFFICE SYMBOL (If applicable) ESM	9. PROCUREMENT INSTRUMENT IDENTIFICATION NUMBER F19628-77-C-0021
8c. ADDRESS (City, State, and ZIP Code) Hanscom AFB MA 01731-5000	10. SOURCE OF FUNDING NUMBERS PROGRAM ELEMENT NO. 61102F; PROJECT NO. 2306; TASK NO J1; WORK UNIT ACCESSION NO. 22

11. TITLE (Include Security Classification)
SEMICONDUCTOR EUTECTIC SOLAR CELL

12. PERSONAL AUTHOR(S)
A. S. Yue, J. G. Yu

13a. TYPE OF REPORT	13b. TIME COVERED	14. DATE OF REPORT (Year, Month, Day)	15. PAGE COUNT
Final	FROM Nov 76 TO Dec 78	December 1986	118

16. SUPPLEMENTARY NOTATION
N/A

17. COSATI CODES		
FIELD	GROUP	SUB-GROUP
09	01	
11	06	

18. SUBJECT TERMS (Continue on reverse if necessary and identify by block number)
In-situ Composite, Multijunction Photovoltaic, Eutectic Composite, Multijunction Solar Cell, Semiconductor Eutectic, Tin Selenide Eutectic

19. ABSTRACT (Continue on reverse if necessary and identify by block number)

Two-phase semiconducting eutectics are potential device-materials. Of these, the SnSe-$SnSe_2$ eutectic was chosen for studies in detail because it consists of multi-p/n-layers of SnSe and $SnSe_2$ semiconductors. Since plasma frequency has not been detected in its infrared reflectance spectrum up to 40 micrometers of wavelength, it suggests that the SnSe-$SnSe_2$ eutectic is a nondegenerate semiconductor.

As-grown $SnSe_2$ single crystals have hexagonal crystallographic structure and show n-type conductivity. Polycrystalline SnSe and $SnSe_2$ films have been successfully prepared in vacuum using a close-space-vapor transport technique.

A single crystal of SnSe grown in a closed tube has a hole concentration of 9.72×10^{17} cm^{-3} and a mobility of 154 $cm^2/sec\text{-}v$ at room temperature. This mobility has relationships of $\mu \propto T^{-1/3}$ for $T < 130°K$ and $\mu \propto T^{-2.25}$ for $T > 130°K$.

20 DISTRIBUTION/AVAILABILITY OF ABSTRACT ☒ UNCLASSIFIED/UNLIMITED ☐ SAME AS RPT ☐ DTIC USERS	21 ABSTRACT SECURITY CLASSIFICATION UNCLASSIFIED
22a NAME OF RESPONSIBLE INDIVIDUAL Joseph J. Hutta	22b TELEPHONE (Include Area Code) (617) 377-4247 22c OFFICE SYMBOL RADC (ESM)

DD FORM 1473, 84 MAR 83 APR edition may be used until exhausted. All other editions are obsolete.

The index of reflection for SnSe single crystals has been determined from a wavelength of 3 micrometers to a wavelength of 40 micrometers and was found to be 3.120 at 3 microns and 3.095 at 15 microns.

An I-V characteristic expressed as $I = I_o \exp(qv/2.08\ KT)$ was measured on a SnSe diode, which exhibits a negative resistance after the breakdown. An indirect band gap of 9.922 eV was obtained from the photo-response measurement on a SnSe diode which is consistent with a value of 0.923 eV, obtained from the optical absorption measurement of thin SnSe wafers.

Although liquid-phase-epitaxial (LPE) growth SnSe film has been prepared successfully at 433°C and at a vacuum of 5×10^{-6} Torr, the preparation of this LPE film on a $SnSe\text{-}SnSe_2$ eutectic substrate has failed due to a large lattice mismatch.

17. COSATI CODES (Continued)

Field	Group
20	12

Table of Contents

List of Figures

List of Tables

Section 1

INTRODUCTION

This is the Final Report describing research performed for the Electronic Systems Division, Air Force Systems Command, USAF Hanscom AFB, MA on "Semiconductor Eutectic Solar Cell" under Contract No. F19628-77-C-0021. The primary objectives are: (1) to grow semiconductor multi-junction eutectics and to investigate their semiconductor heterojunction behavior under the irradiation of electrons and photons and (2) to construct a prototype semiconductor eutectic solar cell and to evaluate its efficiency for energy conversion and the I-V characteristics.

Controlled eutectics for structural application have been extensively investigated. However, very little has been done for nonstructural applications. In recent years, some pioneer works on potential applications of controlled eutectics have been summarized in many review articles [1-4]. In general, these applications are mainly based on the combination of electrical, magnetic, optical, thermal, acoustical, chemical and nuclear properties. Also, electronic devices, such as Magneto Resistors [5], Infrared Detectors [6], light source [7], and Infrared Polarizers [5,8], have been reported. But these devices are still at their infant stages for use.

In semiconducting eutectics, efforts were paid to eutectic systems which consist of III-V semiconductor phases, such as GaAs, InSb, and GaSb, and metal fiber phases [9-12]. The interfaces of these metal semiconductor eutectics are similar to a series of Schottky diode junctions. It is conceivable that another type of semiconducting eutectic consisting of two semiconducting phases could lead themselves into an important role for multi-P/N junction device applications.

In the tin and selenium binary phase diagram (Fig. 1) [13], there are two semiconducting compounds, i.e., tin monoselenide and tin diselenide, and one SnSe-$SnSe_2$ eutectic. The melting temperatures of SnSe, $SnSe_2$ and a SnSe-$SnSe_2$ eutectic are 860°C, 657°C and 625°C, respectively. Figure 2 shows the pressure-temperature projection of the Sn-Se system [14]. The vapor pressures are 64 and 250 Torr at melting points of SnSe and $SnSe_2$, respectively. Technically, these temperature and vapor pressure ranges can be handled without using special equipments. It also has been previously reported that the SnSe compound is a P-type semiconductor with an electronic energy band gap of 0.9 eV [15], the $SnSe_2$ compound is an n-type semiconductor with an electronic energy band gap of 1.0 eV [16], and a unidirectionally solidified SnSe-$SnSe_2$ eutectic has [17] a P(SnSe)-N($SnSe_2$) multilayer microstructure. Because of its simplicity (binary system), achievability (low temperature and pressure) and an anisotype microstructure, the SnSe-$SnSe_2$ eutectic was selected for study.

Since the understanding of semiconductor properties and the development of material processing techniques are the prerequisites for the service of a eutectic as a device material, the objectives of this report are: 1) growing a P-N multilayer SnSe-$SnSe_2$ eutectic; 2) studying the growth variable of the bulk and film crystals of SnSe and $SnSe_2$; 3) developing techniques for diode fabrication (formation of a P-N junction); and 4) investigating semiconductor properties and device characteristics of these compounds.

Instead of diversifying the effort on the broader primary objectives as described in the proposal, the studies were concentrated on the SnSe compound. Figure 3 shows a work scheme for this research.

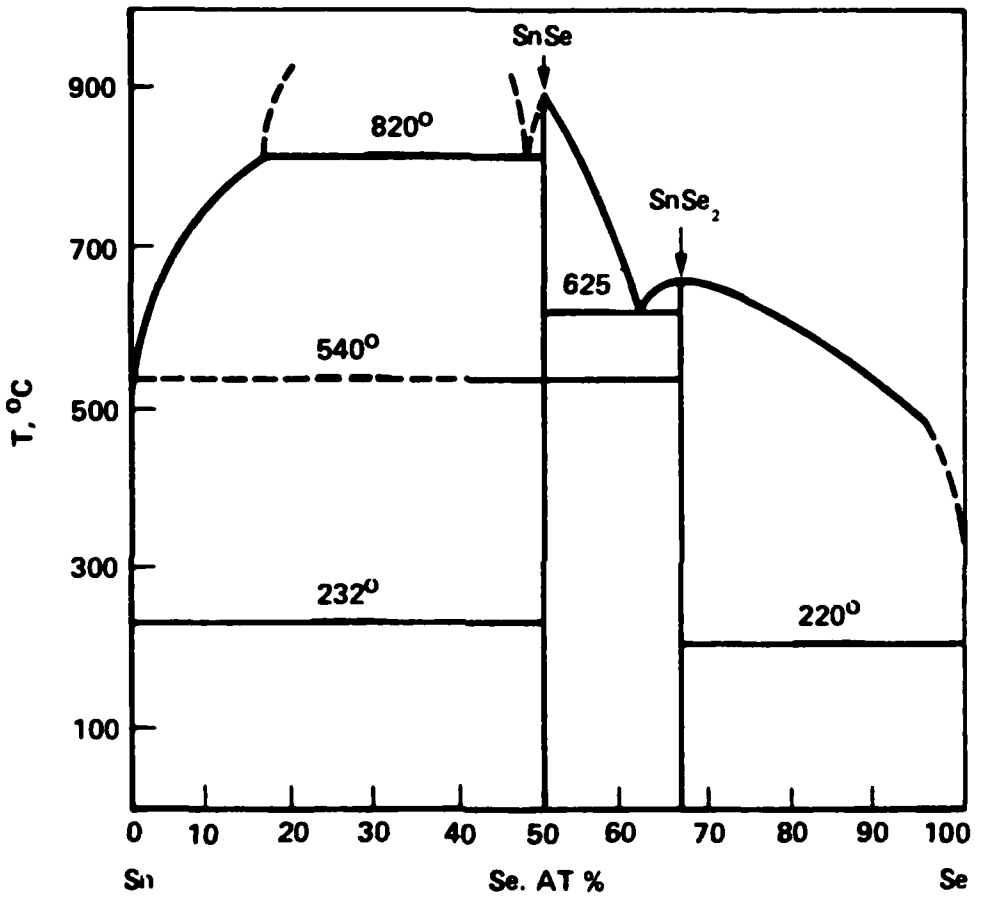

Figure 1. Binary phase diagram of Sn-Se system.

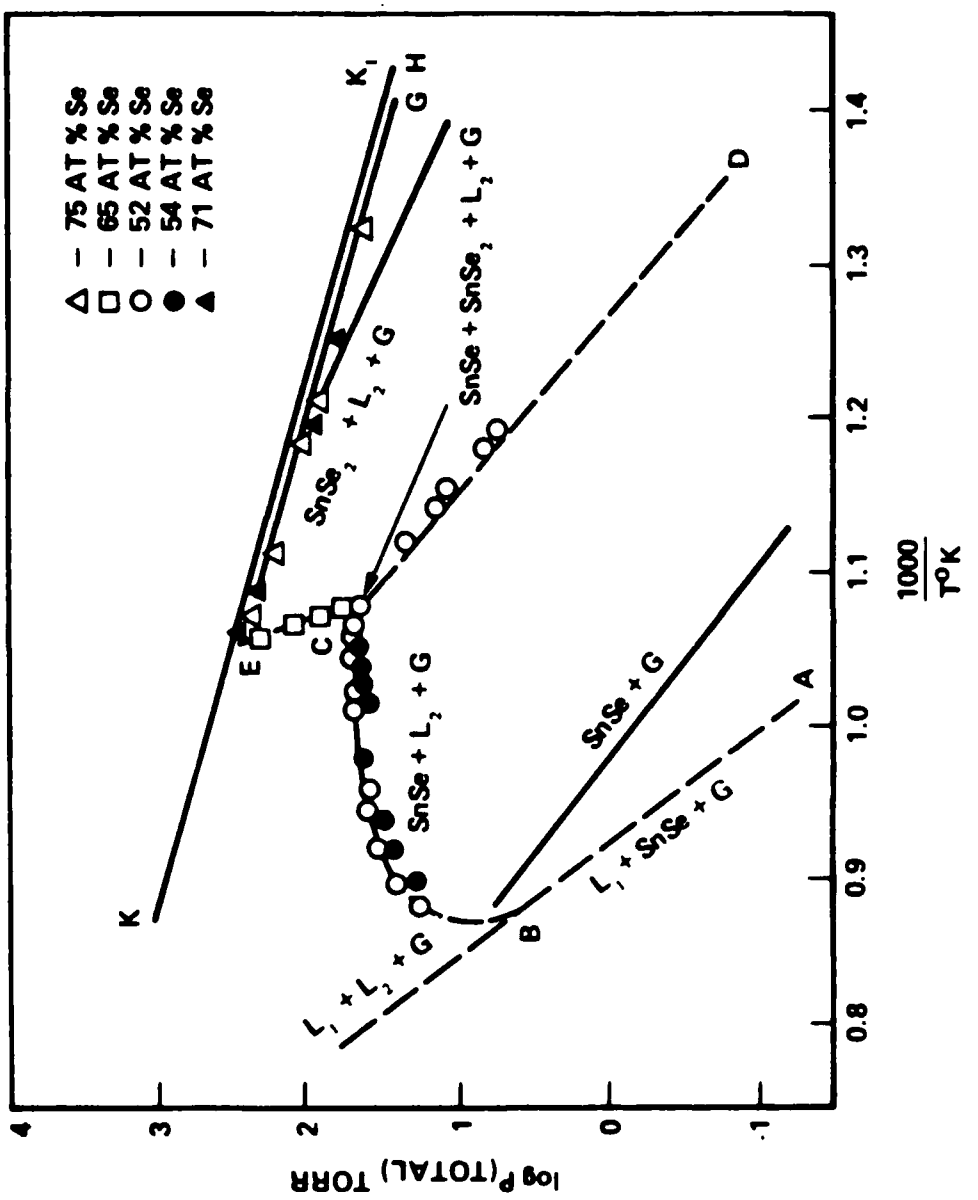

Figure 2. Pressure-temperature projection of Sn-Se system[58].

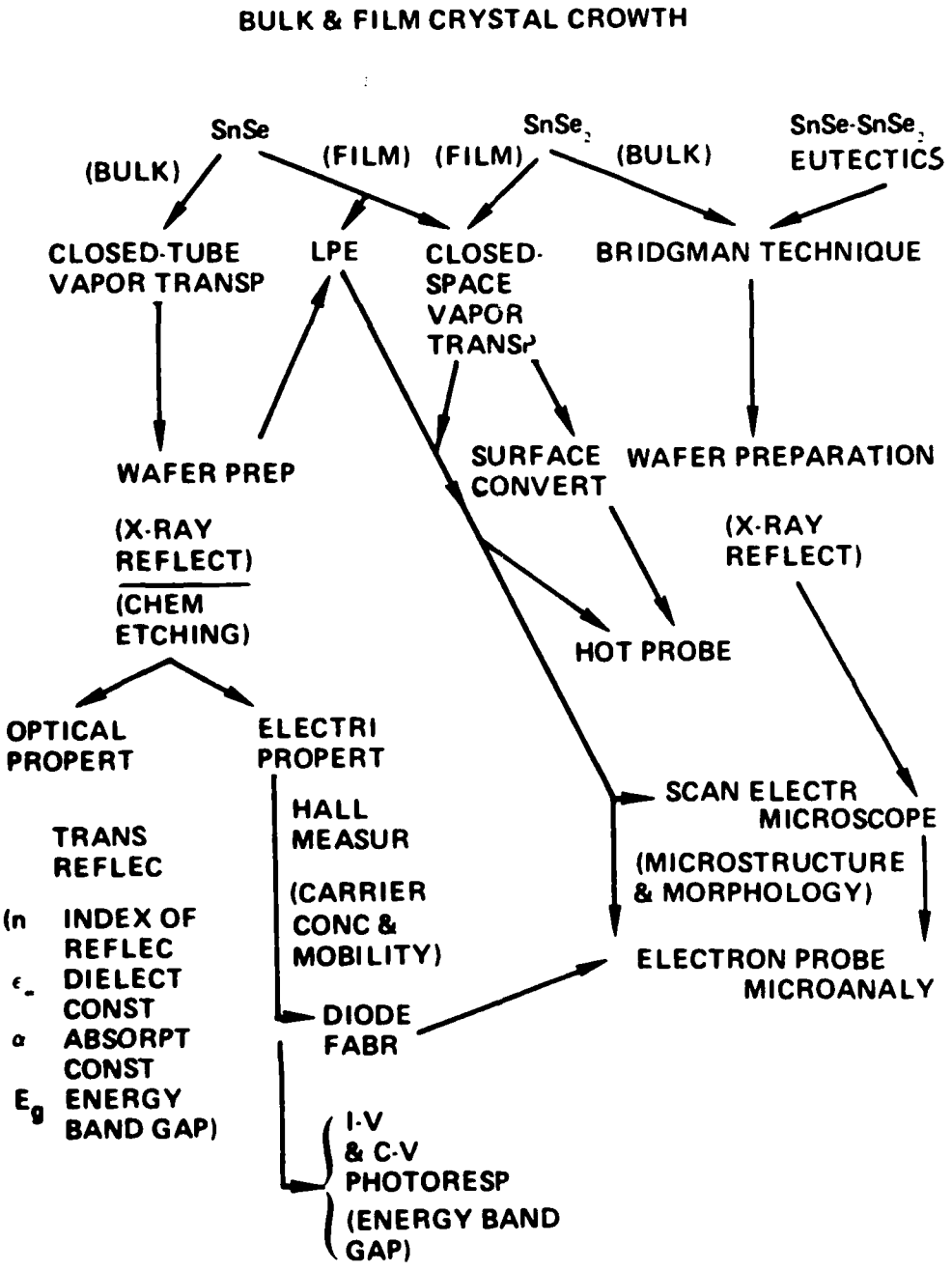

Fig. 3. Work scheme.

SECTION 2

A $SnSe$-$SnSe_2$ EUTECTIC OF MULTI-P/N-JUNCTIONS

A. Growth of $SnSe$-$SnSe_2$ Eutectics

The regions of a solid solubility of SnSe and $SnSe_2$ are not shown in the binary phase diagram, Figure 1. But, an established general rule among III-V, II-VI, and IV-VI compounds is that the cation-rich side of the compound displays N-type semiconductivity and the anion-rich side reveals P-type semiconductivity. Thus, this nonstoichiometric feature of SnSe and $SnSe_2$ causes the multi-P/N-junctions at phase boundaries of the $SnSe$-$SnSe_2$ eutectics.

The growth of the eutectics was conducted in a three-zone furnace (SATEC Systems, Inc.). Figure 4 is the temperature-regulation circuit. The main power comes from a 240 V A.C. source through a magnetic amplifier (saturable reactor) which is regulated by a temperature controller in conjunction with an intermediate magnetic amplifier. Three parallel auto transformers provide three A.C. currents of 0~15 amperes, each of which can be adjusted independently, to each zone of the furnace. The temperature profile in the furnace can be easily manipulated in this manner.

Tin shots of 99.9999 purity (Cominco American, Inc., Spokane, Washington) and selenium shots of 99.999^+ purity (ROC/RIC, Sun Valley, CA) were weighed at 50.9933 wt.% selenium and loaded in a previously

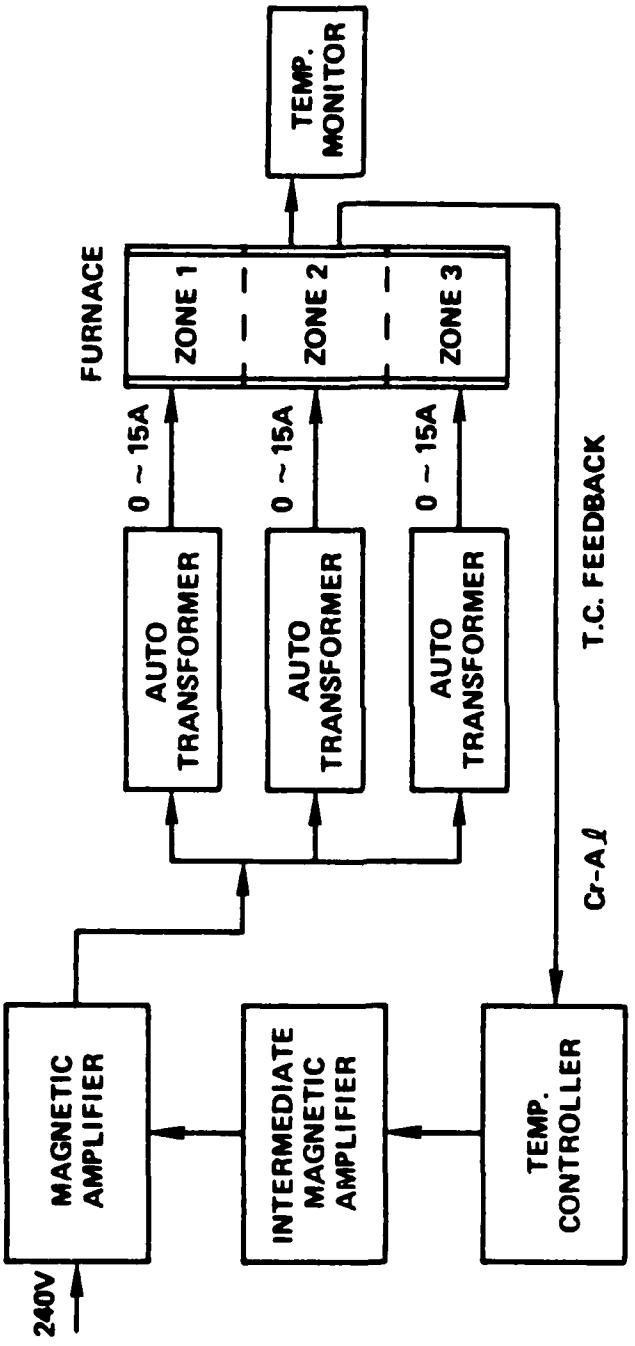

Figure 4. Temperature regulation circuit

cleaned fused-quartz tube with one conical end closed. All the sealed ampoules were vacuum-sealed at a pressure less than 10^{-6} Torr. The quartz tubes were cleaned according to the following steps: washed in a detergent solution, rinsed in D.I. water, soaked in an aqua regia (3 HCℓ:1 HNO_3) for 30 minutes, rinsed in D.I. water and dried in vacuum. Freshly supplied tin shots have shining silver-like surface were used as-received. Those tin shots, which had been exposed to atmosphere, were etched in methanol containing 5% Br_2, rinsed in a stream of methanol from a wash bottle and vacuum dried.

Quartz tubes with 12 mm I.D./13 mm O.D., 15 mm I.D./16 mm O.D., and 18 mm I.D./19 mm O.D. were used in the experimenting as ampoules. Their lengths are approximately 18 cm. They were homogenized at 800°C for 4 days and then slowly cooled. Homogenization at lower temperatures tends to produce voids in the ingots. These voids are believed to be remnants of the unreacted selenium. Homogenization of a SnSe-$SnSe_2$ eutectic charge prepared from the Sn and Se elements was conducted at a temperature higher than the melting point of the $SnSe_2$ (657°C). A longer time was needed for a complete homogenization.

The homogenized charge showed a shining and smooth surface which indicates no reaction between the melt and the quartz-tube wall. The homogenized ampoule was then placed inside a graphite crucible and covered with a graphite cap. A small amount of graphite powder was packed between the tip of the ampoule and the graphite crucible to provide an intimate contact. The graphite crucible minimizes the temperature fluctuation due to its thermal mass and allows a steep

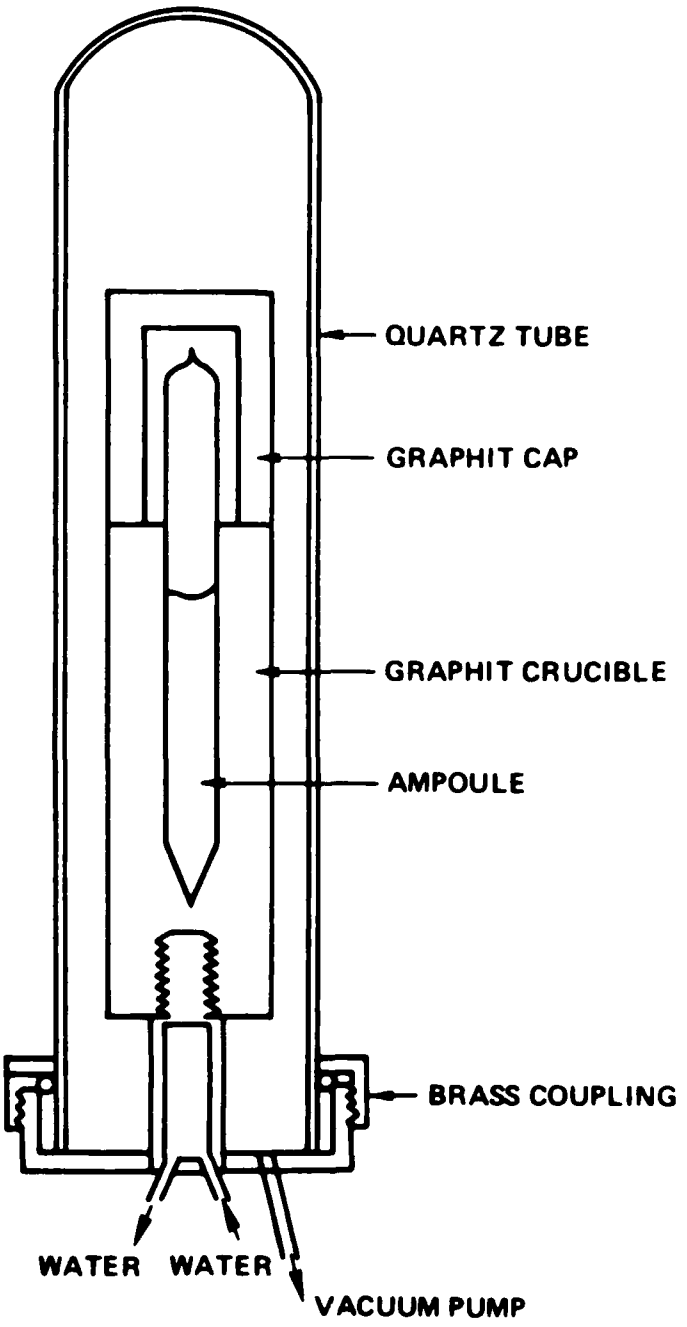

Figure 5. Set up of ampoule and crucible in relative scale.

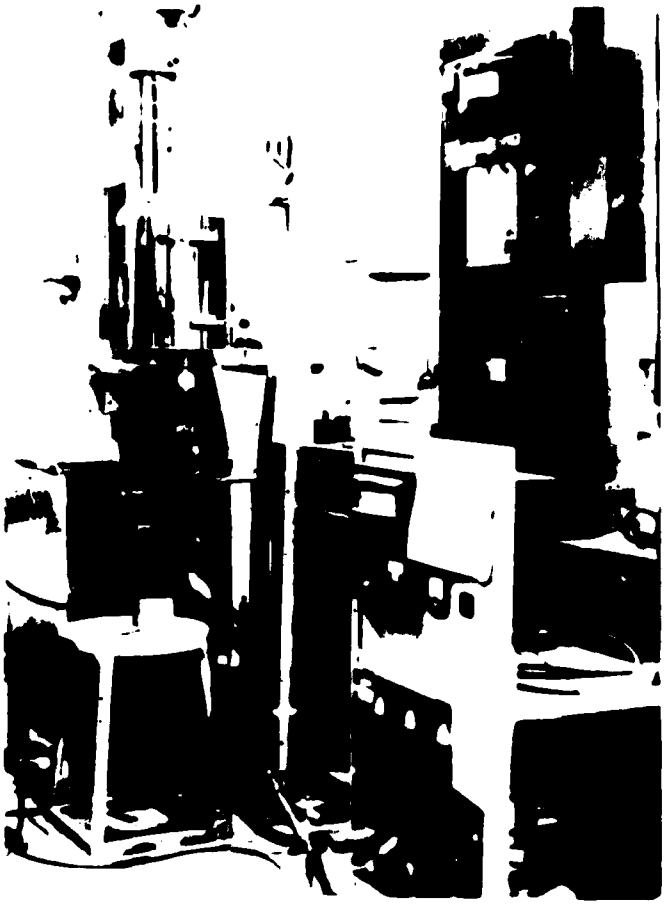

Figure 6. Picture of modified Bridgman growth unit.

Figure 7a. $SnSe$-$SnSe_2$ eutectic of 13 mm diameter

Figure 7b. $SnSe$-$SnSe_2$ eutectic of 18 mm diameter

temperature profile through a water-cooled copper supporter underneath. The graphite crucible is protected from oxidation by inserting it in a large size quartz container under vacuum. The set-up is shown in Figure 5. This set-up is inserted in the three zone furnace which is mounted on a frame of a Lepel crystal growth unit and can be moved up and down at a controlled speed. Figure 6 shows a picture of a modified Bridgman growth unit.

Five $SnSe-SnSe_2$ eutectic ingots were grown at a growth rate of approximately 0.5 cm/hr. and at an estimated temperature gradient of 110°C/cm. Figures 7a and 7b show some of these grown ingots, 13 mm in diameter and 18 mm in diameter, respectively. The ingots of smaller diameters tend to have hollow striations along the grain boundaries of the surface. It is believed that these striations are related to the curvature of the quartz tube. The wetting angle between the Se vapor phase and the tube wall has a smaller value for the case of quartz tube of smaller radius and larger curvature. In other words, the vapor is easier to be trapped between the melt and the wall.

Great care has been taken during the handling of $SnSe-SnSe_2$ eutectic ingots because they are very fragile. A string saw (Laser Tech., Inc., No. Hollywood, CA) was used to slice the ingot into wafers of 150 mil thick, either parallel or perpendicular to the ingot axis. Figure 8 shows the thin $SnSe-SnSe_2$ eutectic wafers.

B. Conformation of Multi-P/N-Layer Structure

A variety of mixed acids have been used to preferentially etch out one of the two phases of the eutectics. It was found that a

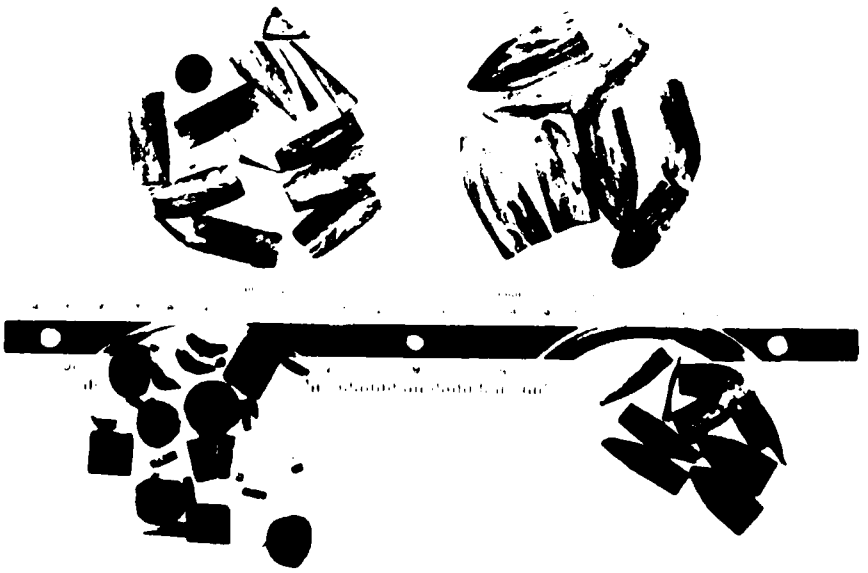

Figure 8. Wafers of $SnSe$-$SnSe_2$ eutectic

solution made of 1 HF and 1 HNO_3 can successfully etch away the SnSe phase in one minute leaving the unetched $SnSe_2$ phase protruding out of the surface as indicated in Figure 9a and 9b. It is believed that the etching process involves an electrochemical reaction between the anode and the cathode of the two phases. During the etching process, an orange color fume was evolved. This fume may be selenium fluoride or hydride which is poisonous. Therefore, it is strongly recommended that the etching procedure must be carried out in a venting hood. The SEM photographs of the longitudinal and transverse sections of the etched eutectics are given in Figures 9a and 9b. In Figure 9b, it shows that the eutectic grain boundaries are made of the SnSe phase and the eutectic grains do not have the same orientation.

The use of a sealed quartz tube hinders the one-dimensional heat extraction during crystal growth. It is expected that an improved crucible design would be able to decrease the number of eutectic grains in the transverse section of an ingot. Since silica has a thermal conductivity value of 0.012 Cal/cm°C and graphite has a value of 0.16 cal/cm°C sec., the use of graphite as a large thermall mass at the lower end of the ampoule is an applausible approach. The X-ray spectrum of the unetched $SnSe_2$ phase at 29 KeV of electron beam is shown in Figure 10. The peaks of the Sn L lines at 3.6 and 3.8 KeV and the Se L line at 1.39 KeV are the strong signals. (Further routine examinations were conducted at an electron beam energy less than 20 KeV.)

The microprobe data of the etched eutectic were compared with those of the grown $SnSe_2$ and those of purchased polycrystalline SnSe

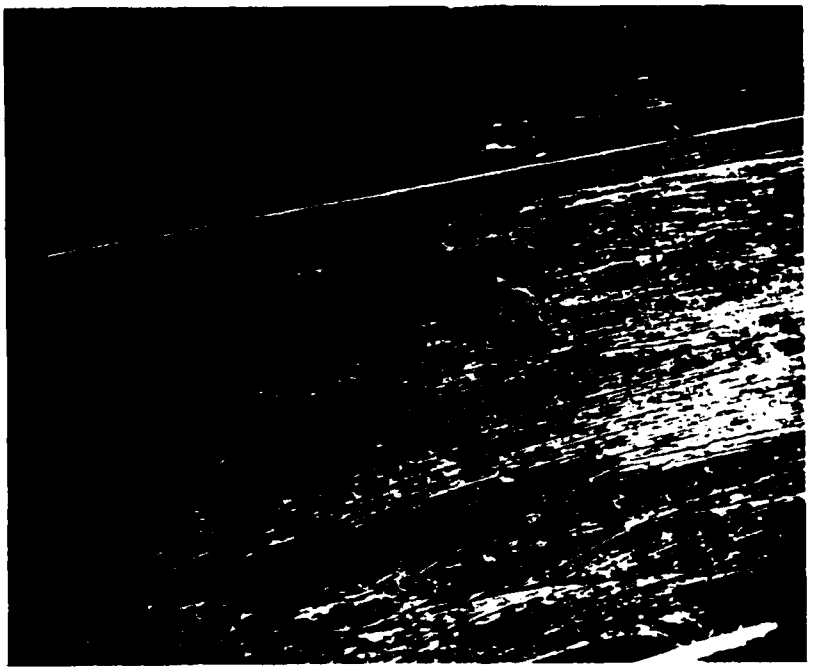

Figure 9a. SEM Picture of longitudinal Section of a SnSe-$SnSe_2$ eutectic (X74)

Figure 9b. SEM Picture of transverse section of a SnSe-$SnSe_2$ eutectic (X115)

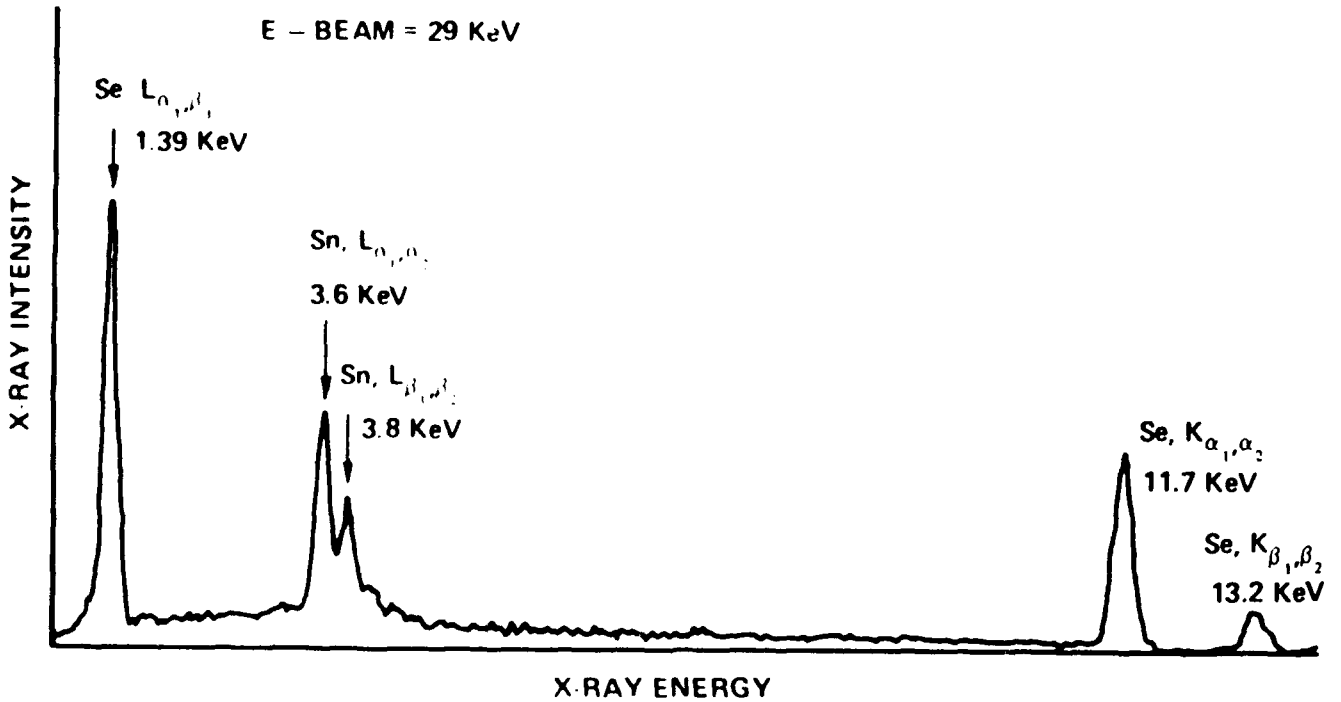

Fig 10 X RAY spectrum of unetched $SnSe_2$ phase of SnSe-$SnSe_2$ eutectic.

(ROC/RIC). Based on these comparisons, it is concluded that the SnSe phase can be preferentially etched away in one minute with a mixed solution of 1 part of HF and 1 part of HNO_3. The immersion of a wafer,cut perpendicular to the growth axis, into this solution will eventually end up with microplatelets of the $SnSe_2$ phase.

Hot probe method was used to check the type of semiconductivity. Although two point probes were used in this case, the contact area is much larger than the size of an individual phase (2~4 micrometer). As a result, only N type conductivity was detected. Since the SnSe-$SnSe_2$ eutectic has (001) of the SnSe phase (orthogonal) parallel to (001) of the $SnSe_2$ phase [18] (hexagonal), both compounds have {001} as their cleavage plane. Ordinary scotch tape was used to cleave layers off the eutectic wafer with their cleaved surfaces parallel to the growth axis. Hot probe measurements on the cleaved surfaces showed the N and P type conductivity. Therefore, it is concluded that the SnSe-$SnSe_2$ eutectic has a multi-P/N-layer structure.

A resistivity measurement with four point probe yielded an average value of 0.6 ohm-cm. So far, there has been no suitable technique to measure the carrier concentration of each phase directly since direct contact to each phase is not possible at the present time. A contactless method using infrared reflection [19] to detect the plasma edge has been tried on the eutectic. At plasma wavelength the reflection becomes metallic and a substantial peak of reflectivity close to unity appears in the reflectance spectrum. The plasma frequency, ω_p, is given by $\omega_p^2 = 4\pi q^2 N/m^* \varepsilon_o$, where q is the electron charge, N is the carrier concentration, m^* is the effective mass and

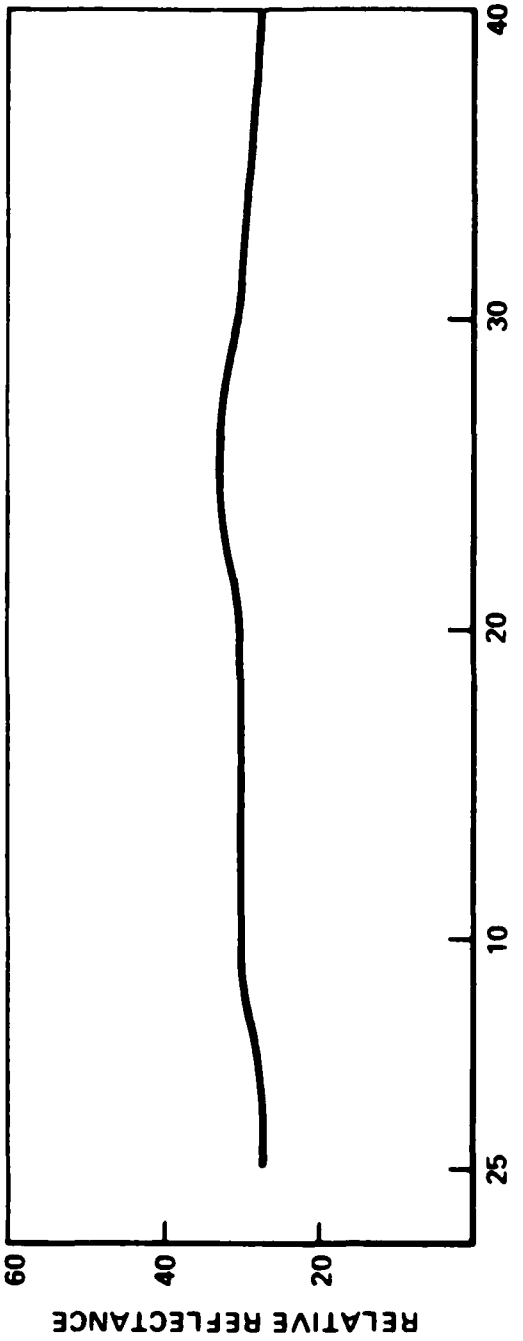

Fig. 11. Reflectance spectrum of $SnSe\text{-}SnSe_2$ Eutectic.

ε_o is the dielectric constant. The plasma edge method has been successfully applied to GaAs [20,21,22], Si [21], Ge [22], PbTe [23], PbS [24], and $Pb_{1-x}Sn_xTe$ [25]. Due to the limitation of practical optical arrangement, this method is generally applicable for heavily doped semiconductors with carrier concentration higher than 10^{18} per cm^3. The infrared reflectivity has been measured from 2.5 to 40 micron wavelength on the eutectic surface of transverse sections using a spectrophotometer (Perkin-Elmer Model 457) in conjunction with a microspecular reflectance accessory (Barnes Engineering Company, Model 126). Figure 11 shows the reflectance spectrum of a SnSe-$SnSe_2$ eutectics. The total reflectivity (R) can be written as $R = aR_1 + bR_2$, where R_1 and R_2 are the reflectivity of SnSe and $SnSe_2$, respectively, and a and b are the percentage of the SnSe and $SnSe_2$ surface areas, respectively. From the reflectance data it is indicated that the carrier concentrations of both phases are not such heavily doped that the plasma edge can be detected within 40 micron of wavelength.

In conclusion, the unidirectionally solidified SnSe-$SnSe_2$ eutectic has been proved that it has multi-P/N-junctions and its constituents are non-degenerated semiconductors.

SECTION 3

$SnSe_2$ SEMICONDUCTING COMPOUND

A. The Nature of $SnSe_2$

Tin diselenide was predicted to have a semiconducting behavior by Mooser and Pearson [26] in 1956 and was later verified through Hall and thermoelectric effect measurements by Bush [27] and Asanable [28] in 1961. Bush also found that $SnSe_2$ has a CdI_2, type C_6, hexagonal structure with lattice parameters a = 3.811 Å and c = 6.137 Å. This structure consists of sheets of hexagonally close-packed identical atoms which are perpendicular to the c axis. This arrangement has the sequence of Se-Sn-Se, Se-Sn-Se,..., along the c axis. Each tin atom is surrounded by six selenium atoms in an octahedral coordination. The cohesion between Se atoms is essentially due to the weak Van der Waal's force. Consequently, the $SnSe_2$ single crystal has (001) basal plane as the cleavage plane.

The optical properties of the $SnSe_2$ semiconductor have been studied by various workers [29-33]. The absorption coefficient has been determined from transmittance and reflection measurements over a wavelength region from visible to infrared. Also the index of refraction was deduced from the interference fringes in the transmittance spectrum. However, the data were inconsistent [33] among the authors. The electronic transitions deduced from absorption data show an indirect energy band gap of 1.0 ± 0.02 (eV) and a direct energy band gap of 2.0 ± 0.1 (eV).

The electronic band structure of the $SnSe_2$ semiconductor has been studied by Au-Yang and Cohen [34] (1969), Fong and Cohen [35] (1972), and William [36] (1973), based on pseudopotential and tight binding methods. William also determined the photothreshold voltage of 5.35 eV and deduced the electron affinity of 4.35 eV for the $SnSe_2$ semiconductor. These studies on the electron band structure of the $SnSe_2$ semiconductor stemmed from the interest on the superconducting properties of transition metal dichalcogenides substantially as a result of intercalation $SnSe_2$ having a layer structure similar to that of transition metal dichalcogenides.

The metal-$SnSe_2$ contact was reported to show polarity-dependent memory switching phenomena by Chun [37] (1974). The current vs. voltage characteristics behavior, either ohmic or reacting, and the switching between two modes can be triggered by biasing over a threshold voltage or applying a pulse of certain current level. The electromigration of the element was observed at the metal-semiconductor interface. More understanding of the electronic properties of the tin-selenium binary system is needed in order to explain the switching phenomena which are generally observed in heterojunction diodes.

B. Preparation of $SnSe_2$ Compound

All the $SnSe_2$ single crystals used to study the optical properties by various workers were grown by the iodine vapor-transport technique in a closed evacuated quartz tube. A mixture of small quantity of iodine and stoichiometric $SnSe_2$ source are placed at the hot end of the ampoule with a proper temperature gradient along the ampoule.

Platelets of $SnSe_2$ are grown at the cold end through the following reaction

$$SnSe_2 + I_2 \rightleftarrows SnI_2 + Se_2$$

SnI_2 and Se_2 are formed in the hot zone and transported to the cool zone where $SnSe_2$ is formed and grown. The iodine acts only as a transport agent and a small amount is needed for growing the $SnSe_2$ crystal. The drawbacks of this technique is that only small size crystals (1 cm^2 x 100 μ) are obtained. This is attributed to a large temperature difference ($\Delta T \simeq 150°C$) between the two zones which promotes a high transport rate and a high nucleation rate.

In this study, a modified Bridgman method as described in Section A of Chapter 2 was used to grow bulk $SnSe_2$ single crystals from the melt. Quartz tubes of 12 mm and 15 mm I.D. and 14 mm and 17 mm.O.D. were used to contain charges weighing from 20 to 38 grams. Two selected compositions were prepared, i.e. stoichiometric composition of Sn and Se with a wt. ratio of 0.751583 and a tin-doped mixture with a wt. ratio of 0.75460. Table 3 lists sizes of the ampoules, weights of tin and selenium, homogenized temperatures and growth rates. The vacuum-sealed ampoules were homogenized for four days at temperatures approximately 135°C above their melting points and then cooled slowly. The homogenized ingots were grown at a temperature gradient approximately 95°C/cm, and a growth rate of

Figure 12a. $SnSe_2$ ingots (12mm X 5 cm)

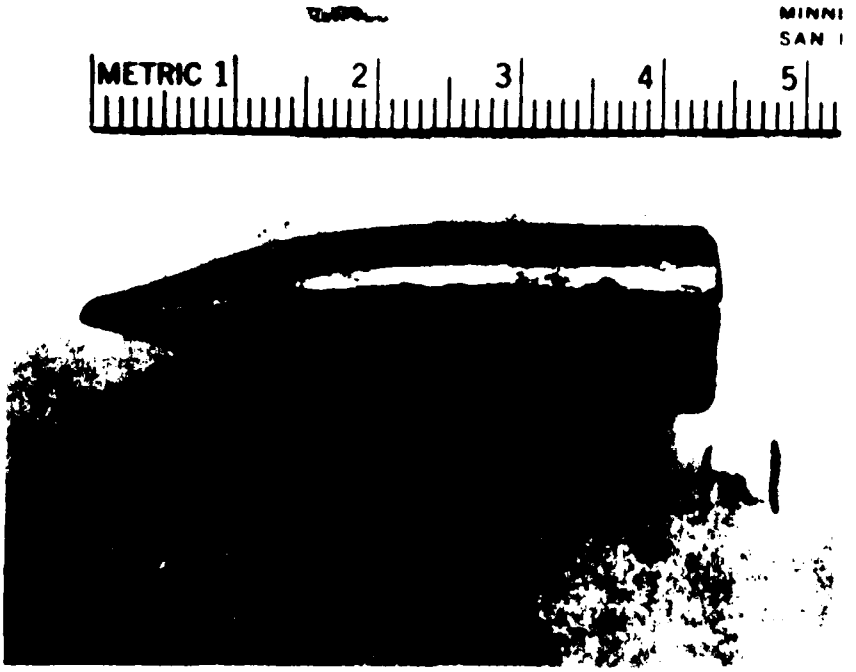

Figure 12b. $SnSe_2$ ingots (14mm X 4.5 cm)

approximately 0.5 cm/hr. All the grown samples were n-type semiconductors. Usually the tip portions about 1.5 cm long are single crystals and the remaining portions of the ingots were polycrystalline materials. Figures 12a and 12b are macrophotographs of $SnSe_2$ ingots of two sizes. The tip-portion single crystal has the c axis perpendicular to the growth axis for ampoules of 12 mm I.D. and has the c axis making 45° with the growth axis for ampoules of 14 mm I.D. Voids frequently appeared in samples homogenized at 700°C.

It was found that the melt can have very large degree of supercooling. At one time, the growth was interrupted and the ampoule with the melt was removed from the furnace. It was found glass-form solid and was formed after solidification in air. This is understandable because the high content of selenium increases the viscosity of the melt and leads to a sluggish diffusion. After the growth exceeding 1.5 cm, the ingots tend to grow in the form of platelets with their c-axes perpendicular to the growth axis. This was due to a decreasing temperature gradient in the melt during growth. A macrophotograph of the transverse section of one $SnSe_2$ ingot can be cleaved along the growth axis.

Single crystals were sliced from the leading portion of the ingots. Figure 14a shows a Laue back diffraction pattern with a 6-fold symmetry. The wafer was cut parallel to the c plane. Single crystalline layers can be cleaved with a scotch tape. Figure 14b is an identical six-fold symmetry Laue pattern of the cleaved layer.

Figure 13. Macrophotograph of the end of one $SnSe_2$ ingot (Diameter = 12mm)

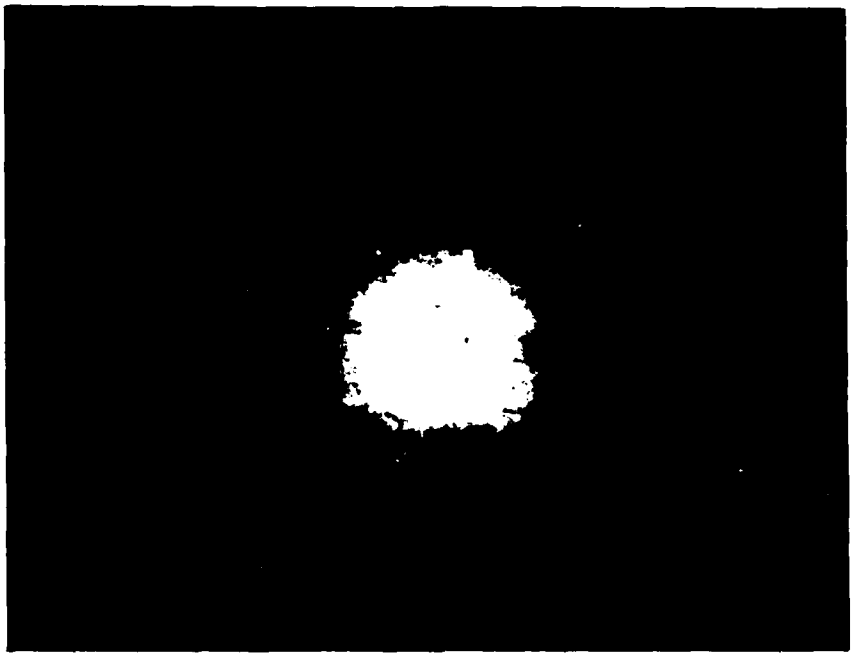

Figure 14a. Laue pattern of cut wafer (001) of $SnSe_2$.

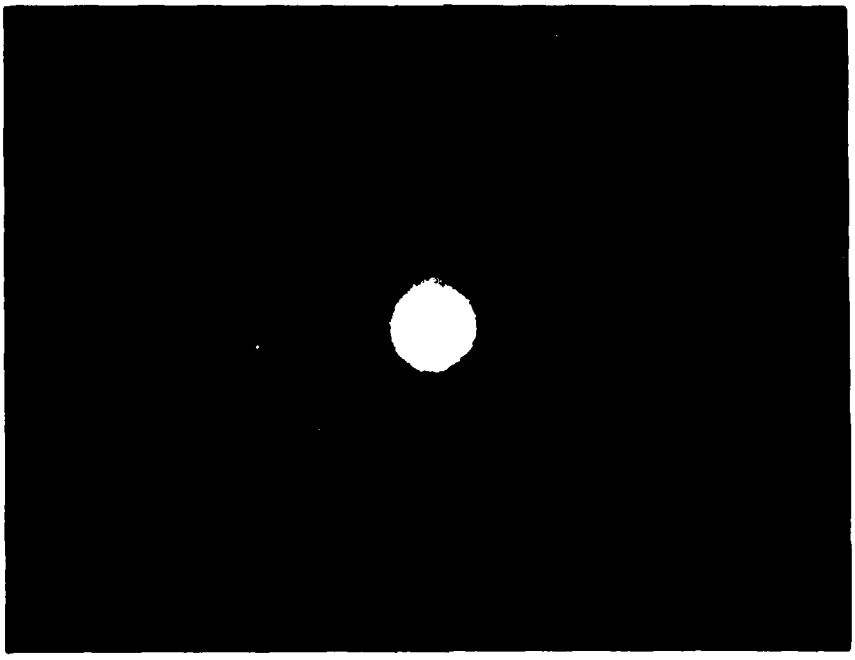

Figure 14b. Laue pattern of cleaved layer of $SnSe_2$.

	SIZE ID/OD (mm)	Sn (gram)	Se (gram)	Sn/Se (wt ratio)	T_{HOMOG}	GROWTH RATE cm/hr	REMARK
1	15/17	8.7257	11.6098	0.7516	700°C	0.5	SINGLE CRYSTAL ABOUT 1.5 cm LONG AT TIP C AXIS: GROWTH AXIS (~45°C)
2	15/17	10.0139	13.2704	0.7546	776°C	0.5	SINGLE CRYSTAL ABOUT 1.5 cm LONG AT TIP C AXIS: GROWTH AXIS (~45°C)
3	12/14	9.9987	13.3035	0.7515	806°C	0.5	SINGLE CRYSTAL ABOUT 2 cm LONG. C AXIS ⊥ GROWTH AXIS
4	12/14	8.7745	11.6747	0.7516	806°C	0.6	SINGLE CRYSTAL ABOUT 2 cm LONG. C AXIS ⊥ GROWTH AXIS
5	12/14	8.7207	11.6031	0.7516	806°C	0.5	SINGLE CRYSTAL ABOUT 2 cm LONG. C AXIS ⊥ GROWTH AXIS
6	12/14	8.7745	11.6747	0.7516	806°C	0.6	SINGLE CRYSTAL ABOUT 2 cm LONG. C AXIS ⊥ GROWTH AXIS
7	15/17	16.3675	21.6903	0.7546	810°C	0.5	SINGLE CRYSTAL ABOUT 1.5 cm LONG. C AXIS ⊥ GROWTH AXIS
8	15/17	16.1685	21.7904	0.7420	810°C	0.5	SINGLE CRYSTAL ABOUT 1.5 cm LONG. C AXIS ⊥ GROWTH AXIS

Table 1. Growth data of $SnSe_2$ single crystals.

The elongated, diffracted spots were induced in the pattern due to the presence of thermal strain upon solidification. The resistivity, ρ, measured on the wafers using four point probe ($\rho=2\pi SV/I$) has values from 0.7 ohm to 1.2 ohm/cm, where S is the distance between the points, V and I are the voltage and current, respectively.

The I-V characteristics of two metal points in contact with the $SnSe_2$ wafer shows reactification for both directions of biasing. Reflectance measurements on the wafer show no plasma frequency edge for wavelength up to 40 microns. It is concluded that the $SnSe_2$ crystals are not degenerated.

C. Preparation of $SnSe_2$ Film

a. Dissociation Problem of $SnSe_2$

Physical vapor deposition of $SnSe_2$ film was tried at a vacuum of 5×10^{-6} Torr on a glass substrate. The brown color film is nonconductive. The major component of the film is selenium. It is well known that dissociation of a compound during heating usually occurs and the different sticking coefficients of the vapor species generally exist in thermal vapor deposition. Techniques such as flash evaporation, electron-gun evaporation, multi-source evaporation and hot-wall evaporation are developed to overcome the difficulty. Films of II-VI and IV-VI compounds can be more successfully deposited from the vapor phase than those of III-IV compounds, because the latters have a large difference in partial pressure between Group III and V elements.

In the work of Karakhanova [38] (1967) on the determination of the dissociation pressure of solid tin diselenide in vacuum, selenium was found in the apparatus. A reaction, $nSnSe_2$(solid) $\rightleftarrows$ nSnSe(solid) + nSe(gas) was assumed for temperatures below 614°C. The total selenium pressure was calculated by the "dew point" method which is given as

$$\log P(\text{mm Hg}) = -\frac{5032+300}{T(°K)} + 7.962 \pm 0.20 \quad .$$

However, the consideration of a partial pressure over the SnSe solid apparently should be included wherever the actual experiment is performed. Mass spectrometer data showed that the vapor over solid SnSe is composed of SnSe, Se_2 and Sn_2Se_2 [39]. The actual vapor pressure over solid $SnSe_2$ measured by a membrane null manometer [40] has the following relationship

$$\log p(\text{mm Hg}) = -\frac{9718}{T(°K)} + 12.052 \pm 88.387 \times 10^{-6}$$

$$+ 285.673 \times 10^{-6} \times \left(\frac{1}{T(°K)} - 1.1209\right)^2$$

A congruent evaporation was assumed for the temperature range of 580°C-638°C. The following two reactions were proposed in their work:

$$SnSe_2(\text{solid}) \rightleftarrows SnSe(\text{gas}) + 1/2Se_2(\text{gas})$$

$$SnSe_2(\text{solid}) \rightleftarrows SnSe_2(\text{gas})$$

It is not completely understood as to which reaction is actually taking place during sublimation. In the experiment of conventional physical-vapor-deposition of $SnSe_2$ through sublimation, the residue had a sponge-like conducting mass with a metallic color. Also it was found that the conductivity of the surface of the $SnSe_2$ wafer had been changed from an original N-type to a P-type semiconductor after heating the compound in vacuum at 400°C for 20 minutes. This apparently is a result of a deficiency in selenium after heating the compound in vacuum even for a short period of time. It is concluded that 1) the reaction during evaporation was not congruent and 2) the most reasonable reaction was

$$SnSe_2(\text{solid}) \rightleftarrows n\,SnSe(\text{gas}) + \left(1 - \frac{n}{2}\right) Se_2(\text{gas})$$

$$+ (1-m-n)\,Sn(\text{solid}) + m\,Sn(\text{gas})$$

After this evaluation, it is understandable that the indexes of reflection data determined by Kostyshin [29] who prepared the $SnSe_2$ film by the vapor deposition technique were far off from those data reported by other workers [33].

b. A Semiequilibrium Approach - The Close-Space-Vapor-Transport Method without Transport Agent

Based on the above analysis, we have adopted the close-space-vapor transport method for preparing the $SnSe_2$ film. Attempts have been made to achieve a quasi-equilibrium condition such that a reaction can take place on a substrate.

The close-space-transport method introduced by Nicoll [41] (1963) and by Stirtl [42] (1963) has been successfully applied to grow epitaxial layers of elemental and compound semiconductors, such as Ge (Tramposh, 1969) [43], Si (May, 1965) [44], GaAs (Semiletov, 1967) [45], GaP (Sajjn and Maslov, 1965) [46], InP (Nicolau, 1972) [47], CdS (Yoshikawa, 1975)[48], ZnSe (Hovel, 1969) [49], ZnS (Nicoll, 1965) [41], CdTe (Michell, 1975) [50] and $Hg_{1-x}Cd_xTe$ (Tufte, 1969) [51], Cohen-Solal, 1971) [52]. This method is based on the chemical transport reactions extensively studied by Schafer [53] (1962,1971) and Nitsche [54] (1967). The source and substrate wafers are separated from each other by a very small distance, which should be less than 0.1 of their diameter according to Nicoll [41]. The source and substrate can either be in an isothermal condition or have a moderate temperature difference which mainly depend on a specific system involved. A transport agent is generally used in each case. However, there was no transport agent used for the deposition of $SnSe_2$ in this experiment.

A high purity graphite slab (2.5 x 8 x 0.2 cm) was used as a heater inside the vacuum system. A chromel-alumel thermocouple inserted into the graphite slab was connected to a temperature controller (Lees & Northrup Speedomax H and Ser. 60) which controls the A.C. output of a SCR power supply. After the reactification, D.C. current was fed into the graphite heater.

A piece of short quartz tube, 12 mm I.D., 13 mm O.D. and 3 mm in height, a graphite heater was used to separate the source and the substrate. Small $SnSe_2$ wafer, prepared by the Bridgman method, was loaded inside a quartz tube as a source. The substrate wafer was sitting on the top of the quartz tube and completely covered the tube opening. A second thermocouple was placed in contact with the substrate to monitor the temperature.

The above arrangements provide a semiclosed system when the mean free path is considered and provide a hot wall to decrease the undesired loss of material through deposition.

c. Results

It has been observed that noticeable sublimation of $SnSe_2$ started at 330°C and at a vacuum of 5×10^{-6} Torr. The best film was obtained with a source temperature of 350°C and a substrate temperature of 150°C which can be adjusted by varying the length of the quartz spacer.

No intention was made to measure the electrical properties except to identify the type of conductivity. $SnSe_2$ film of P type conductivity has been deposited on SnSe (P-type) single crystal substrate. It was not possible to deposit an N-type $SnSe_2$ film on SnSe substrate. However, N type $SnSe_2$ has been deposited on the eutectic substrate. Since there was no set-up for controlling the substrate temperature, polycrystalline film was obtained at 170°C substrate temperature.

The composition of the $SnSe_2$ film on SnSe substrate was checked using an electron beam microprobe. Figure 15 shows a plot of X-ray

intensity versus energy for the film and the substrate. Figure 16 is a SEM micrograph of the film on a substrate. The main conclusion from this observation is that the composition of a P-type $SnSe_2$ film can be retained by using a close-space-vapor-transport method. However, an N-type $SnSe_2$ film has not been made.

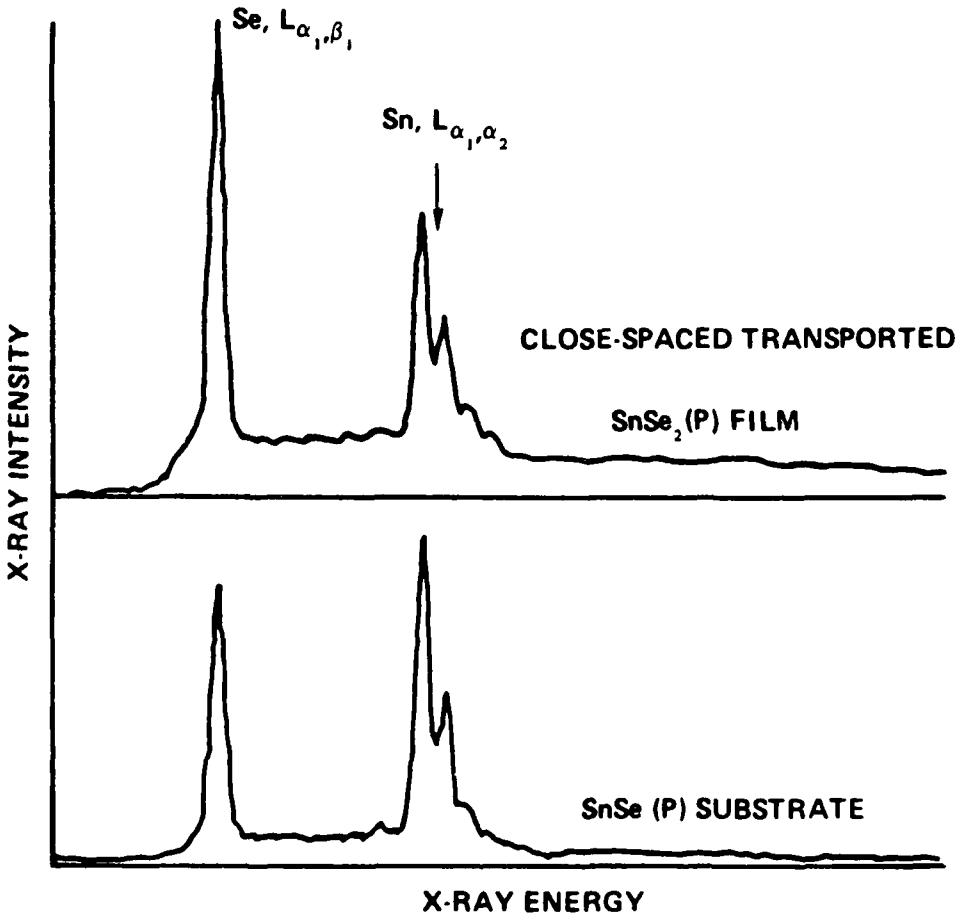

Fig. 15. Electron probe microanalysis of close-spaced-grown $SnSe_2$.

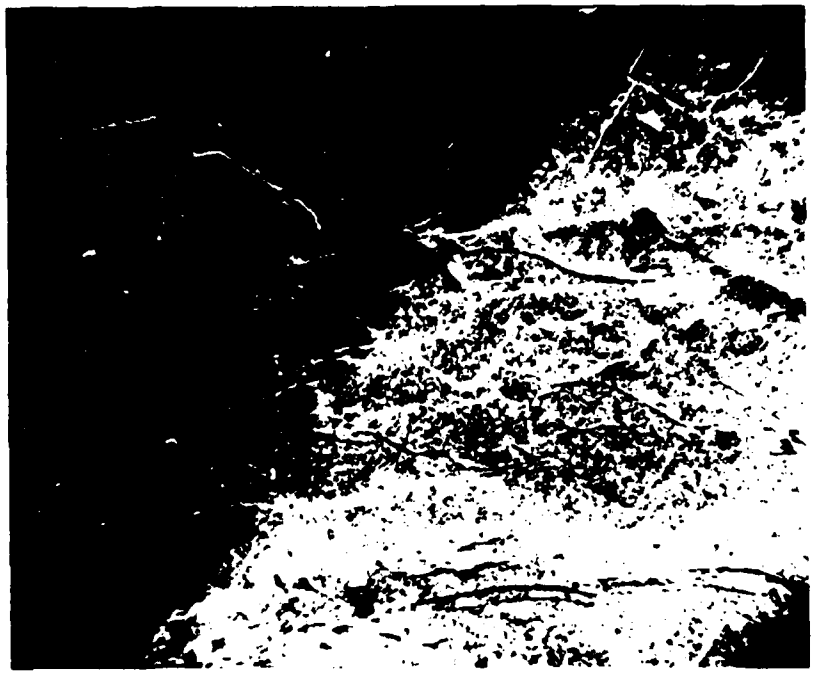

Figure 16. SEM (Secondary electron mode) micrograph of $SnSe_2$ (P) film (white area) on cleaved SnSe (P) Single crystal substrate (X 500)

SECTION 4

SnSe SEMICONDUCTING COMPOUND

A. The Nature of SnSe

Tin monoselenide has an orthorhombic structure with lattice parameters a = 4.46 A, b = 4.19 A and c = 11.57 A [55]. The as-grown SnSe crystal is a P-type semiconductor [56] and the N-type SnSe crystal was obtained by doping it with antimony [58]. The electronic band gap of the SnSe semiconductor was determined to be 0.9 eV at room temperature through the optical absorption measurement.

Optical properties of SnSe were investigated in detail by Mochida [59] who shows a relationship between polarization and optical properties. The anisotropic optical absorption was used to deduce three energy band gaps corresponding to three crystallographic directions. The aluminum contacts on SnSe also show polarity-dependent memory switching effect in the current versus voltage relation. This switching effect was also observed in $SnSe_2$ [37].

B. Growth of Single Crystal of SnSe from Vapor Phase

Both Bridgman and iodine vapor-transport methods used by previous workers for the preparation of SnSe single crystals. In the Bridgman method, heat transfer was apparently retarded due to a double sealing of the quartz ampoule containing the crystal because the ampoules frequently crack upon cooling. Although iodine

vapor transport method was reported to be able to grow crystals in a relatively short period, the crystals are limited in sizes (1 cm^2 area and 100 μ thick). Therefore, the close-tube-vapor-transport method without a transport agent was selected for preparing SnSe single crystal in this investigation.

a. Principles of Vapor Growth

The close-tube-vapor-transport method utilizes the equilibrium reaction between evaporation of a source material at a higher source-temperature and the condensation of the transported material at a lower growth temperature. Evaporation of the vapor phase takes place through sublimation at a temperature lower than the melting point of the source material. The difference in equilibrium vapor pressures between the source site and the growth site produces the transport of the vapor phase. A transport agent *sometimes* is used to provide a transport mechanism for source material having low vapor pressures. Figure 17 shows the arrangement of an ampoule in the close-tube-vapor-transport method. According to Schieber [60], single crystals usually form under the following conditions: 1) $L/D > 7$ where L is the distance between the growth site and the source and D is the diameter of the ampoule and 2) $0.6 < (P_1-P_2)/P_2 < 6$ where P_1 and P_2 are the equilibrium vapor pressures at source temperature and growth temperature, respectively.

b. Experimental Method and Determination of Proper Supercooling

In an earlier preliminary experiment on the recrystallization of SnSe at 840°C for three weeks, it was found that part of the SnSe

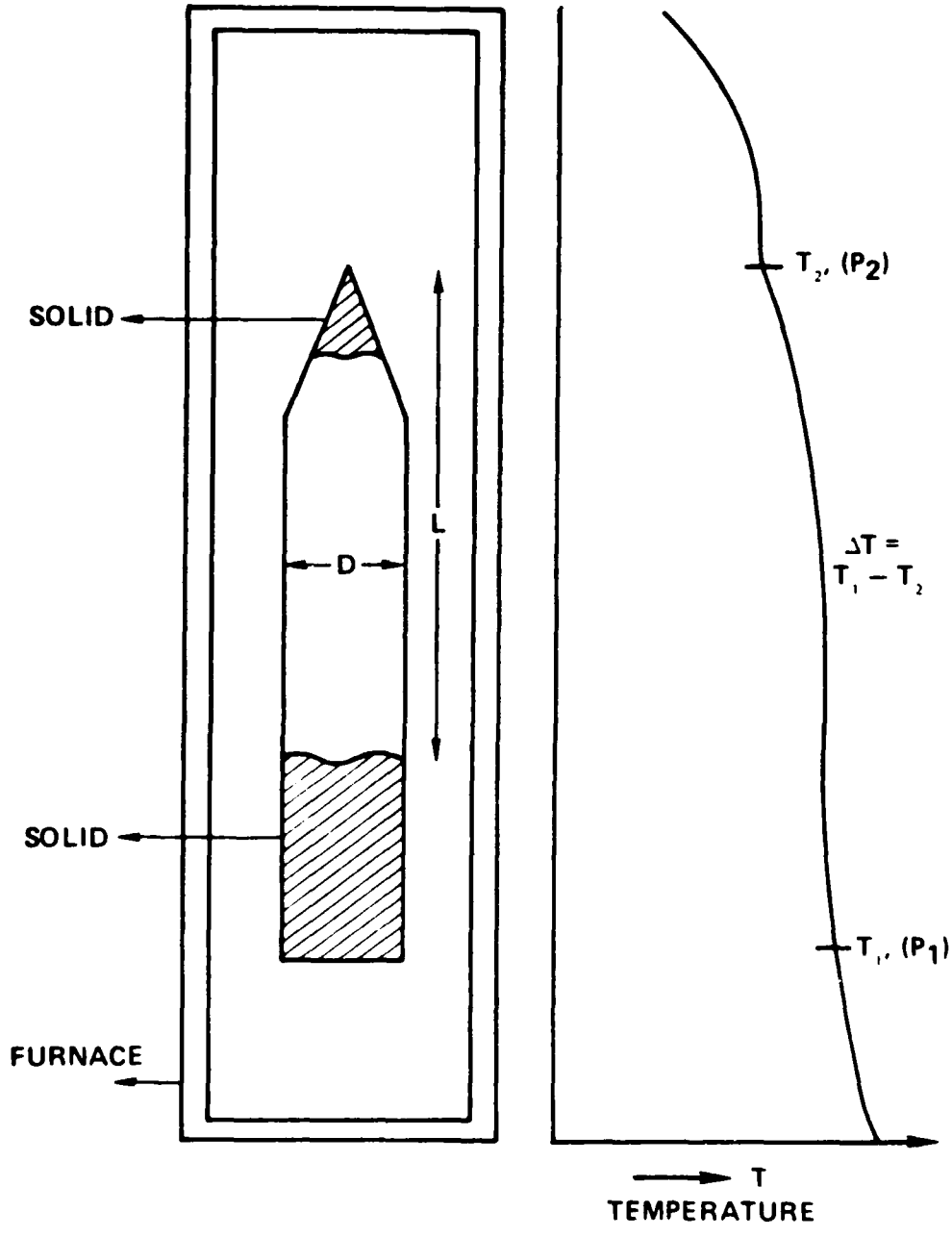

Fig. 17. Closed-tube-vapor transport through sublimation T_1 = the source temperature, T_2 = the growth temperature and ΔT = the supercooling.

had been transported vertically from the bottom of an ampoule to its top. Figure 18a shows the recrystallized SnSe and Figure 18b shows the transport-grown SnSe single crystal. Their single crystalline nature was confirmed by X-ray Laue back diffraction patterns and the electron beam microprobe analysis. The vapor-transport was due to an unproper setting of the temperature profile over the ampoule for recrystallization. Later, efforts were devoted to determine the proper supercooling $\Delta T = T_1 - T_2$ required for the formation of single crystals. In growing single crystals from the melt, a larger supercooling is maintained at the solid-liquid interface. In the case of growing single crystals from the vapor phase, a small supercooling should be maintained to avoid spurious nucleation. In vapor growth, the growth rate is slow, as a result of small supercooling.

Two preliminary experiments were performed to determine a proper supercooling which would produce a good quality single crystal.

An ampoule, 18 cm long and 16 mm in I.D. was loaded with tin and selenium shots at a stoichiometric composition of SnSe and was vertically set in a three-zone resistance-wound furnace. The temperature T_1 of the bottom of the ampoule and the temperature T_2 of the top of the ampoule were monitored by two chromel-alumel thermocouples. The temperature was raised to approximately 900°C for two days for homogenizing the charge. Growth started as the temperature T_1 was lowered to 850°C and T_2 lowered to 850°-ΔT°C. It was found that a supercooling of 150°C was able to transport all the solid

Figure 18a. Recrystallized SnSe

Figure 18b. Transport-grown SnSe (X 2.6)

charge (approximately 30 g) to the top in one week. The growth started with crystals of platelets and then changed to columnars. Figure 19a shows a transported crystal and Figure 19b shows the end view of the crystal. From Figure 19b, it was evident that single crystals were formed in columns. Initially, a supercooling of 150°C yielded a large quantity of nuclei. As the growth process proceeded, the supercooling decreased to a level such that single crystal growth in the form of columnar striation was favorable.

In the second run, an ampoule, 18 cm long and 13 mm I.D./15 mm O.D., was set inside a cylindrical firebrick with two monitoring thermocouples. After homogenization, supercooling was 25°C for the first ten day period and 38°C for the next five-day period to increase the growth rate. The temperature profile is shown in Figure 20a, and the grown single crystal is given in Figure 20b. The ampoule cracked during cooling and oxidation took place. Consequently, a thick nonconductive coating was formed on the exterior of the crystal. The cleaned surface, as shown in Figure 20b, is clear and shining. The two vapor-transport-grown SnSe crystals are P-type, nondegenerate semiconductors.

Results of the two preliminary experiments indicated that a supercooling around 30°C is needed to grow SnSe single crystal in the close-tube-vapor-transport method. Therefore, in the final stage of crystal growing, we employed T_1 = 800°C, T_2 = 770°C, and ΔT = 30°C, for the vapor-transport growth. Three ampoules, 18 cm long and 18 mm I.D./20 mm O.D. of tin doped, stoichiometric and selenium doped compositions were grown in a single run. The temperature history

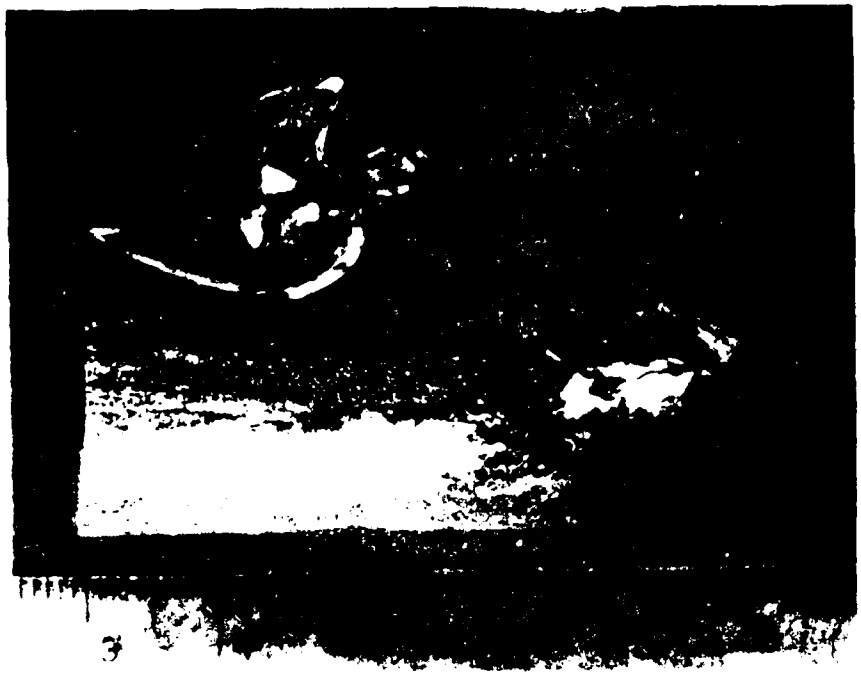

Figure 19a. The side view of columnar growth ($\Delta T = 150^{o}C$).

Figure 19b. The end view of columnar growth, ($\Delta T = 150^{o}C$)

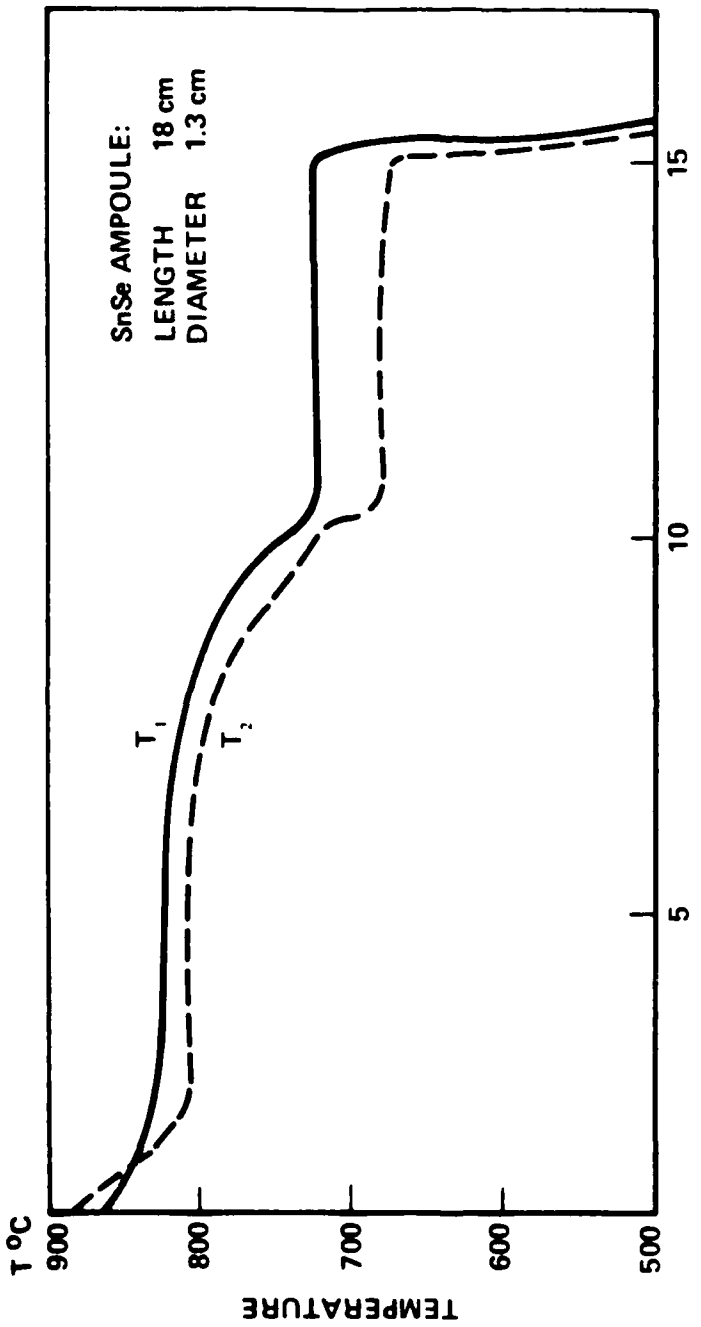

Fig. 20a. The temperature history of the 2nd run of vapor-transport.

is shown in Figure 21. After sixteen days of growth, one third of the source material (SnSe) was transported in the Sn-doped ampoule, about one-fifth of source material was transported in ampoules of stoichiometric and selenium-doped compositions.

c. Results of Vapor-Growth SnSe Single Crystals

Table 4 lists the experimental data of the three ampoules that were grown using the vapor-transport-growth method. Figures 22a, b, and c show the SnSe crystals. During the two days of slow cooling from 880°C to room temperature, the Sn-doped ampoule tended to have Sn-rich vapor species which was thermodynamically in equilibrium with a pure tin melt at a lower temperature. Therefore, a N-type SnSe film was formed on the surface. However, in the Se-doped ampoule, the equilibrium vapor species at temperatures lower than the eutectic temperature contained SnSe and $SnSe_2$ molecules in thermodynamic equilibrium. In comparison with the equilibrium vapor pressures of SnSe and $SnSe_2$ solids, the vapor of the Se-doped SnSe ampoule was supercooled with respect to $SnSe_2$ and the $SnSe_2$ was deposited during cooling. Depletion of selenium leads to an N-type surface on the top of the left crystal. The equilibrium total vapor pressures of SnSe (line AB) and $SnSe_2$ (line CD) are shown in Figure 23. The vapor pressure of an ampoule containing Se-doped SnSe at growth temperature (substrate) is represented by point 4 which is supercooled with respect to $SnSe_2$. The deposited $SnSe_2$ film has a hexagonal

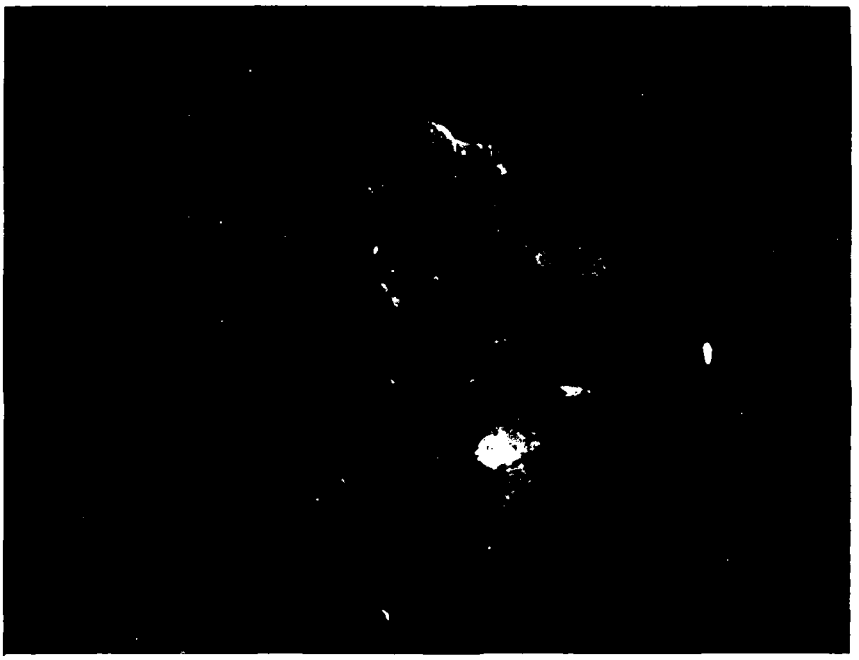

Figure 20b. Oxidized SnSe Single crystal ($\Delta T = 25^{\circ}C$)

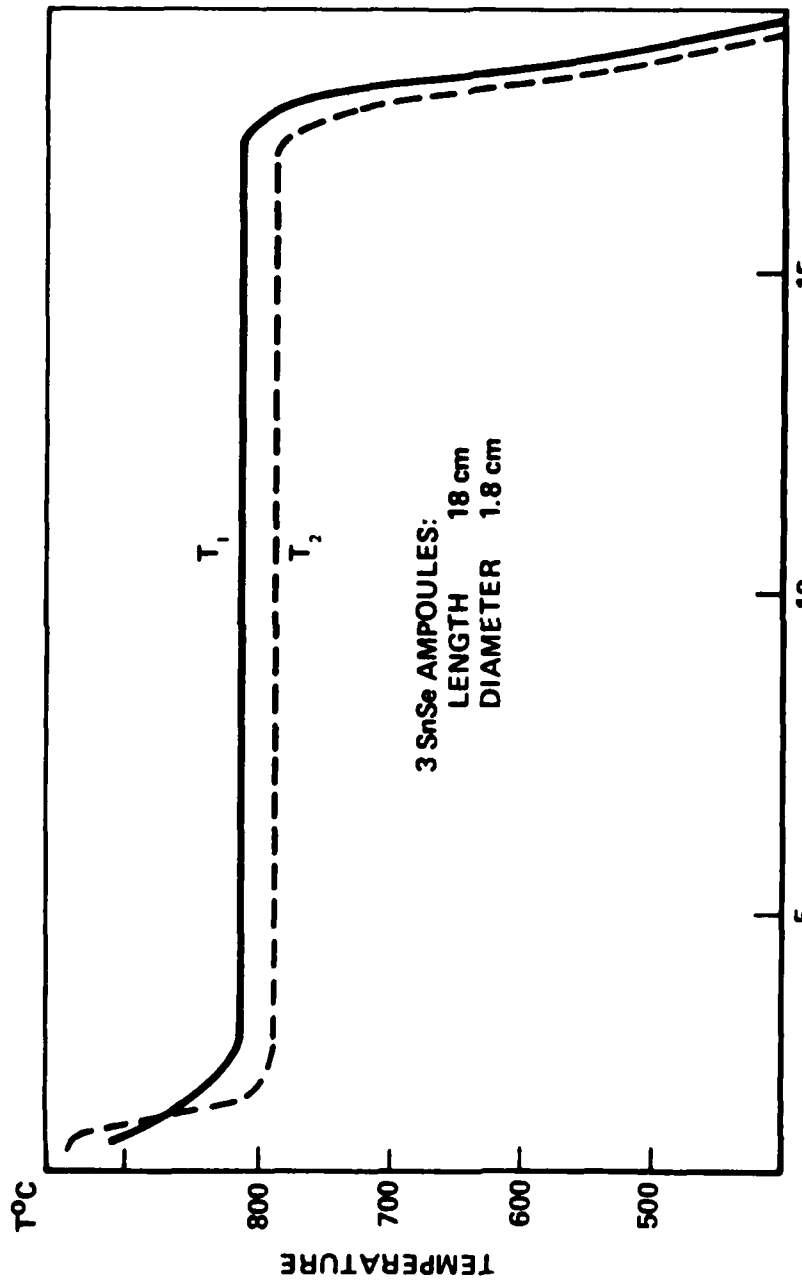

Fig. 21. Temperature history of vapor transport of three ampoules $\Delta T = 30^{\circ}C$.

Figure 22a.

Figure 22b.

Figure 22c.

Figure 22a, b, c. SnSe ingots of Sn-doped, stoichiometric and Se-doped.

Table 2

Growth data of SnSe single crystals.

Ampoule #	A	B	C
Charge (grams)	Sn = 25.088	Sn = 28.234	Sn = 24.984
	Se = 18.780	Se = 18.793	Se = 16.687
Sn/Se wt. ratio	1.509	1.503	1.497
	(Sn-doped)	(stoichiometric)	(Se-doped)
Wt. of transport-grown SnSe (grams)	14.442	8.533	9.764
Wt.% transported	34.62%	18.14%	23.43%
Type of conductivity of transported SnSe	P-type single crystal, N-type surface at lower end.	P-type single crystal.	P-type interior single crystal, N-type film of $SnSe_2$ on surface.
Type of conductivity of left charge.	P-type crytals, N-type surface at upper end.	P-type crystals.	P-type crystals, N-type surface at the upper end.

spiral growth habit which is shown in Figure 24. The composition is further confirmed by the microprobe analysis data. Its X-ray spectrum of the transported SnSe at 800°C and Bridgman Method grown $SnSe_2$ are plotted in Figure 25 for comparison.

C. Wafer Preparation

After growth, one end of the ampoule was cut with a diamond saw. The crystal was carefully removed and mounted on a plastic plate with one of the following materials: paraffin, stearic acid, beeswax or phenyl salicylate. It was found that phenyl salicylate is the most suitable cement for this work because of its easy cleaning and low fluent temperature of 45°C. Laue back diffraction patterns were taken on three spots along the length of the ingot. Figure 26 shows a pattern taken on the surface of a SnSe crystal. It was confirmed that transport grown crystals were single crystals. Also it was found that several (cm^3) large single crystals were formed in the untransported portion of the source material. These crystals were sliced into wafers along either the (001) surface plane or a surface plane parallel to the c-axis (i.e.$\perp$(001)) with a 0.008 inch diameter diamond-powder-impregnated wire saw (Laser Technology, Inc., N. Hollywood, CA.)). Wafers, 0.030 to 0.050 inches thick, were cut and subseqently lapped using a shaking table. Polishing was done by hand, using 3 μ, 1 μ and 0.5 μ $A\ell_2O_3$ powders on a nylon cloth. One batch of polished wafers is shown in Figure 27. Its Laue patterns of (001) and $\perp$(001) are shown in Fig. 28a and 28b, respectively.

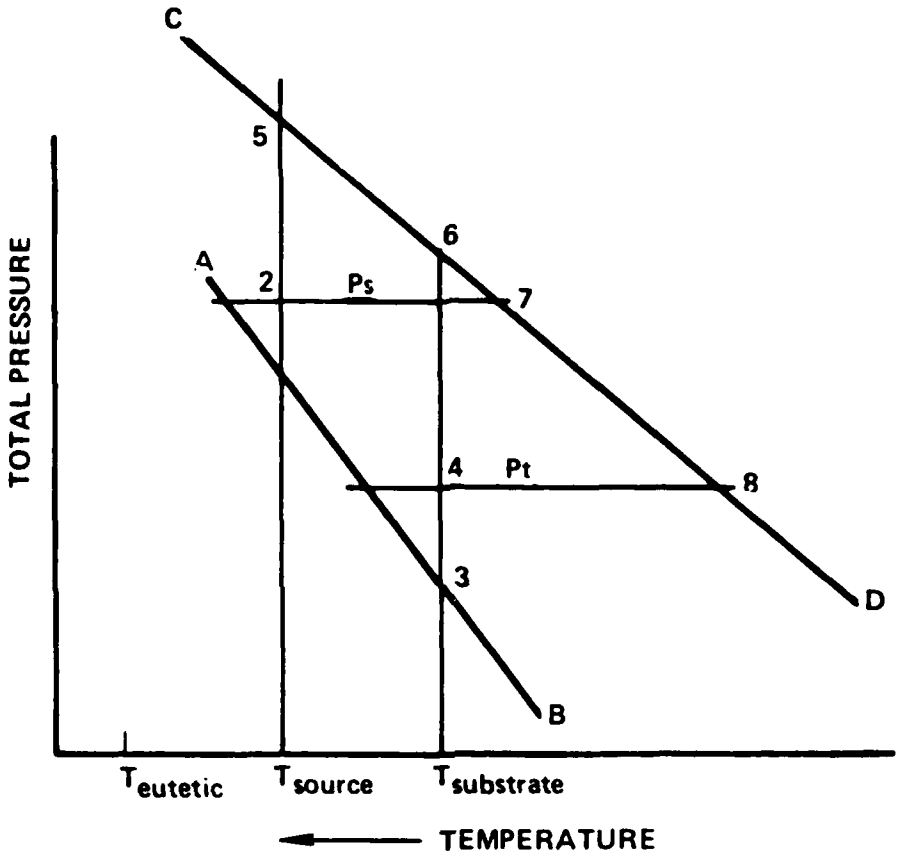

Figure 23. Equilibrium pressures of SnSe (AB) and $SnSe_2$ (CD) and vapor pressure of ampoule C (Se-doped) at source temperature (2) and substrate temperature (4).

Figure 24. Spiral growth of $SnSe_2$ in Se-doped SnSe ampoule at temperature below eutectic temperature (X123)

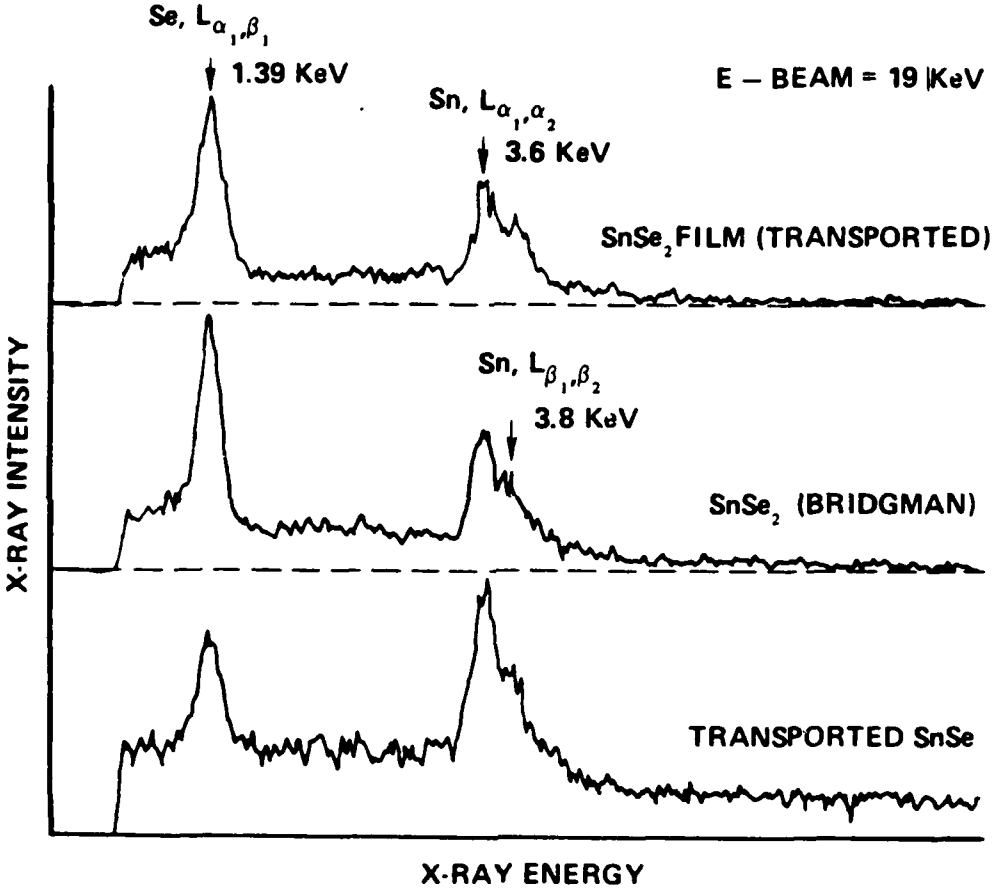

Fig. 25. X-RAY spectrum of transported SnSe (Se doped).

Chemical etching was followed to remove the damage after mechanical polishing. Two drops of Br_2 solution in 30 ml of HBr can oxidize the surface of the SnSe wafer which is shown in Figure 29. The color of the oxidized surfaces changes from metallic white to pink-brown, then royal blue and metallic white again. The oxidized surfaces were cleaned using 40 ml of HCℓ with one drop of Br_2 solution. The surface changed its color reversely. The chemically cleaned wafers were used for alloying tin film to form a diode and as substrates for liquid-phase-epitaxial growth of SnSe films.

D. Some Electronic and Optical Properties of SnSe Single Crystal

a. Hall Measurement and Four-Point-Probe Method

The electrical resistivity of the SnSe wafers was measured by means of the four-point-probe method. A constant current source was applied to the two outer probes and the voltage was read between the two inner probes. The resistivities of SnSe wafers are listed in Table 5. The correction factor for wafer thicknesses has been taken into account in the calculation [61].

The resistivity measured on a plane containing $\vec{c}$-axis generally has a higher value than that measured on (001) plane.

Hall measurement was conducted on the (001) plane of a transport-grown SnSe wafer cut from crystal B over a range of temperature from 30°K to 300°K. A refrigerator of Air Product was used in conjunction

Figure 26. Back Laue diffraction pattern of the Surface of SnSe Crystal.

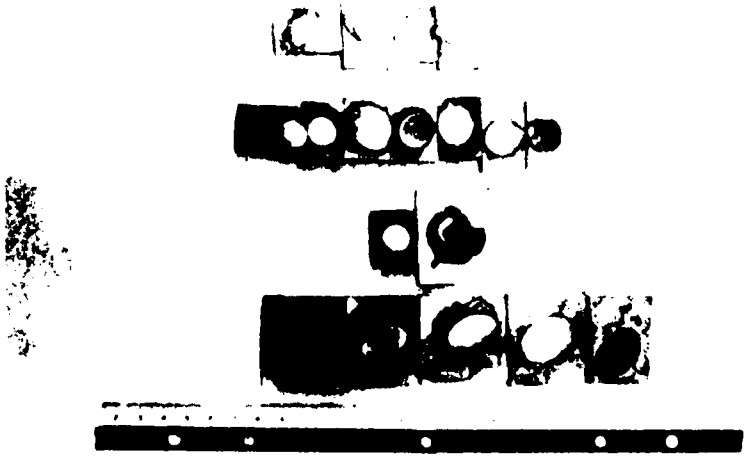

Figure 27. Polished Wafers.

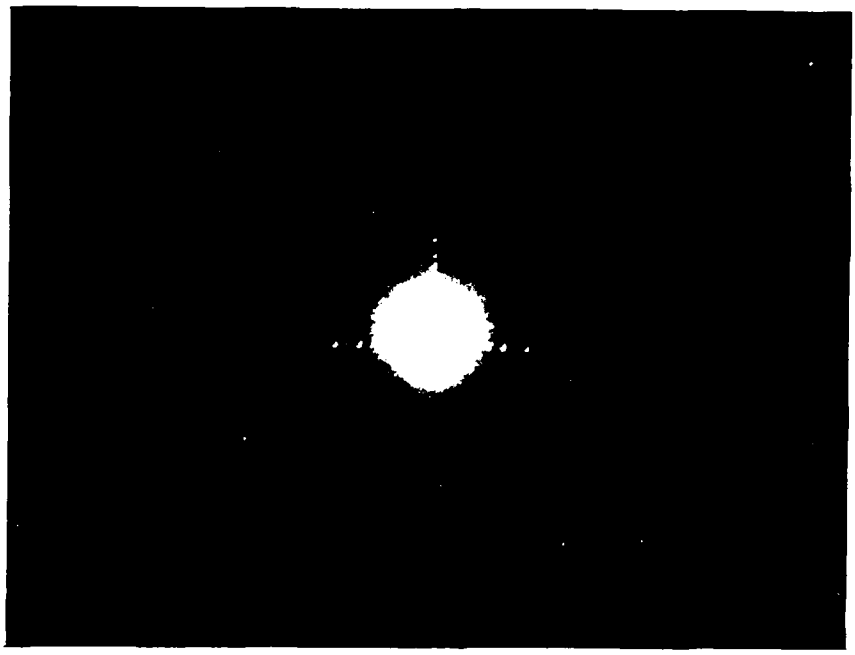

b-crystal

Figure 28a. Laue pattern of (001) of SnSe 30 Kev. 40 mA. 1 1/2 hr.

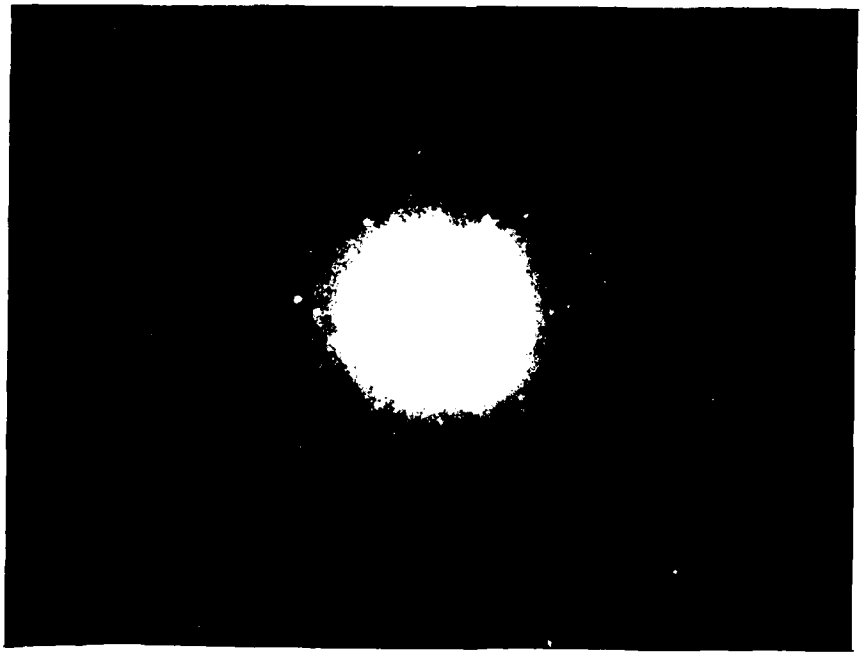

a-crystal

Figure 28b. Laue pattern o f SnSe plane II [001].

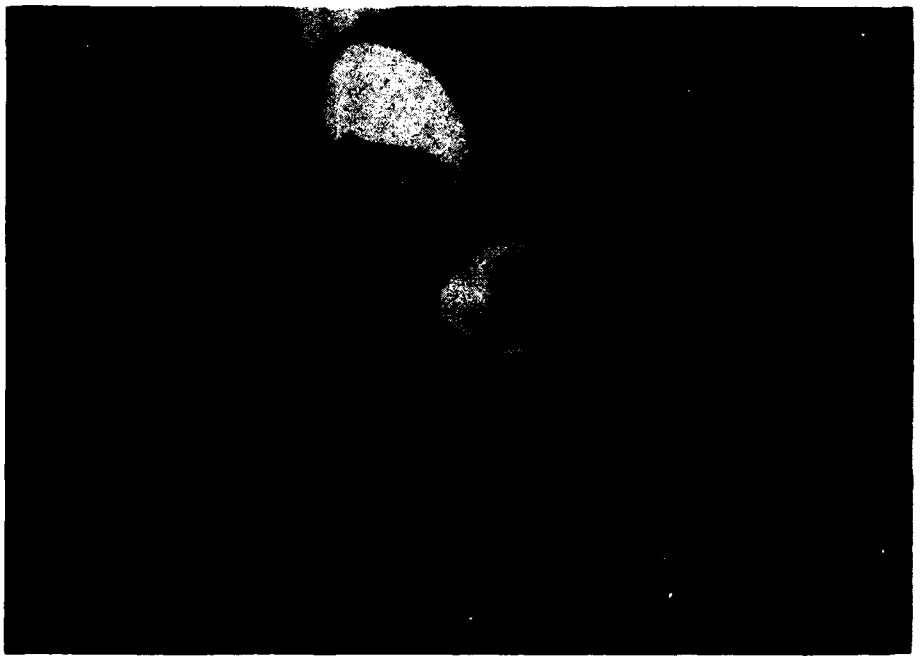

Figure 29. Chemical etched SnSe Wafers.

Table 3

The resistivities (ohm-cm) of SnSe Wafers.

Crystal A Tin-doped SnSe				Crystal B Stoichiometric SnSe				Crystal C Selenium-doped SnSe			
Transported		Sublimed (left over)		Transported		Sublimed (left over)		Transported		Sublimed (left over)	
||(001)	⊥(001)	||(001)	⊥(001)	||(001)	⊥(001)	||(001)	⊥(001)	||(001)	⊥(001)	||(001)	⊥(001)
0.044	0.064	0.041	0.065	0.0415		0.052	0.058	0.059		0.050	0.062

with a duwar. Four gold wires were welded to the edge of the wafer using pure indium as the solder. Curve tracer indicated that the contacts were ohmic. A constant current source of 18.5 mA and a magnetic field of 5 KGauss were applied in the Hall measurement. Table 6 lists the data of the Hall measurement. The resistivity was calculated using $\rho = (\pi d/2\ \ell n2)(V_{DC}/I_{AB} + V_{BC}/I_{AD})f$ where d is the wafer thickness, V is the measured voltage, and I is the applied current. The correction factor f was obtained from Van der Pauw's f function [61]. The Hall coefficients were calculated using equation $R_H = 10^8\ V(B)\ t/I\ B$ where V is the Hall voltage and B is the magnetic field and t is the thickness. The mobility $\mu = \bar{R}/\bar{\rho}$, where $\bar{R}$ and $\bar{\rho}$ are the average Hall coefficients and resistivity, respectively, and carrier concentration $n = 1/\bar{R}e$, where e is the electronic charge, are also listed in Table 6.

The temperature dependence on carrier concentration and conductivity are shown in Figure 30a and the temperature dependence on mobility is shown in Figure 30b. From Figure 30a, it is evident that the carrier concentration has a small variation with temperature. However, the mobility is proportional to $T^{-2.24}$ for $T > 130°K$ and to $T^{-1/3}$ for $T < 130°K$. The former relation indicates that a lattice scattering is dominant at higher temperatures. As the temperature is cooled below 130°K, the lattice vibration is frozen such that impurity scattering is the main mechanism for the scattering process.

b. Reflectance and Transmittance Measurement

Several thin wafers of SnSe were sliced with surface parallel to (001). The thicknesses of polished wafers were measured using a dial thickness gauge after optical measurements. Figure 31 shows samples with thicknesses varying from 5×10^{-3} cm to 20×10^{-3} cm. The transmittance was measured from 0.85 to 2.5 micrometer wavelength in a Perkin-Elmer spectrophotometer, Model 137G, which is a dual beam infrared spectrophotometer. A Barnes model 126 micro-specular reflectance unit was used in the reflectance measurement. The six-mirror beam condensing system has an incident angle of 20°. The compensator was set to give the reflectance of a freshly deposited Aℓ film a value of 98% at 2.5 micrometers. Figure 32 shows one of the transmittance and reflectance curves of SnSe. The absorption coefficients, α, are calculated using the following equation

$$\alpha = \frac{1}{d} \log\{\frac{[1-R]^2}{2T} + [(\frac{1-R^2}{2T}) + R^2]^{1/2}\}$$

which is deduced from a transmittance equation, $T = (1-R)^2 e^{-\alpha d} / (1-R^2 e^{-2\alpha d})$, where α is the absorption coefficient, d is the thickness and T, R are the transmittance and reflectance, respectively.

The absorption coefficients vs. photon energy of five samples are shown in Figure 33. The average value, $\bar{\alpha}$, is also shown in the same figure. Noticeable deviation starts to appear at photon energy less than 1.2 eV. Probably, the surface conditions of these specimens are the main factor causing this deviation. For near the fundamental

Table 4

Hall measurement data.

Temperature T (°K)	Inverse Temp. (1000/T(°K)	Resistivity ρ (Ω-cm)	Conductivity σ (Ω^{-1}-cm^{-1})	Mobility μ (cm^2/sec V)	Carrier Concentration (cm^{-3})
30	33.33	5.203×10^{-3}	192.00	1591.19	7.55×10^{17}
54	18.52	5.62×10^{-3}	177.94	1143.3	9.72×10^{17}
68	14.71	5.85×10^{-3}	170.94	1308.9	8.16×10^{17}
89	11.24	6.58×10^{-3}	151.98	314.4	3.04×10^{18}
130	7.7	7.04×10^{-3}	142.13	1018.58	8.72×10^{17}
210	4.76	21.70×10^{-3}	46.08	318.88	9.03×10^{17}
256	3.91	31.12×10^{-3}	32.14	214.07	9.37×10^{17}
300	3.33	41.60×10^{-3}	24.04	154.46	9.72×10^{17}

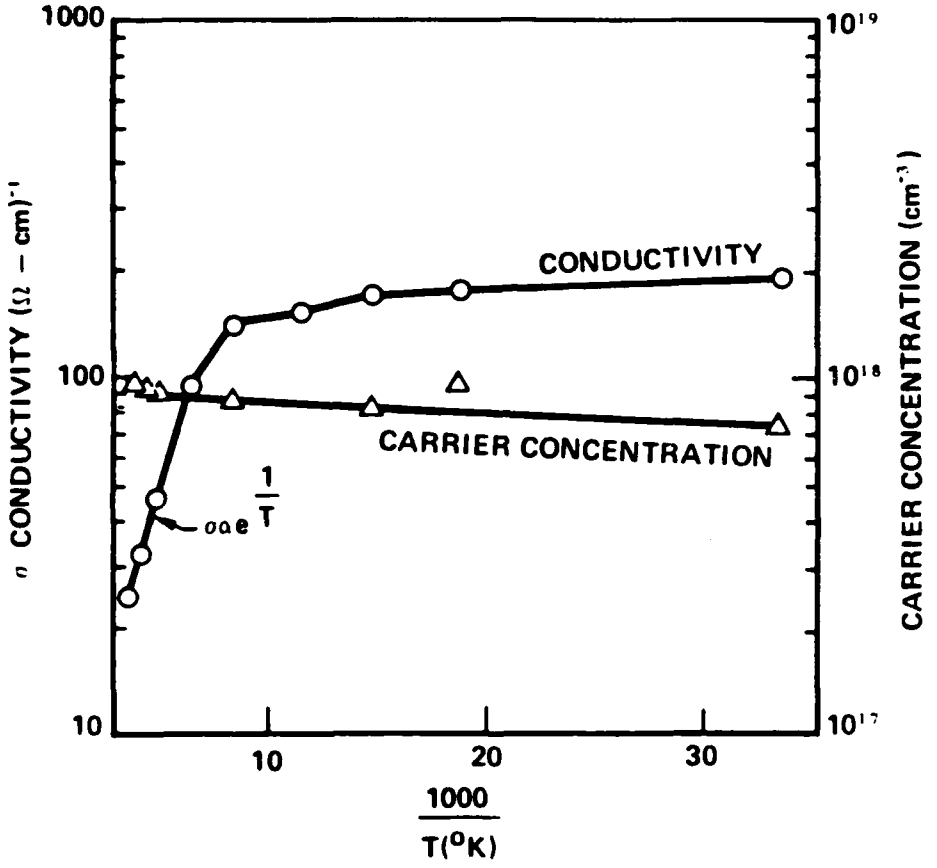

Fig. 30a Carrier concentration and conductivity vs 1/temperature.

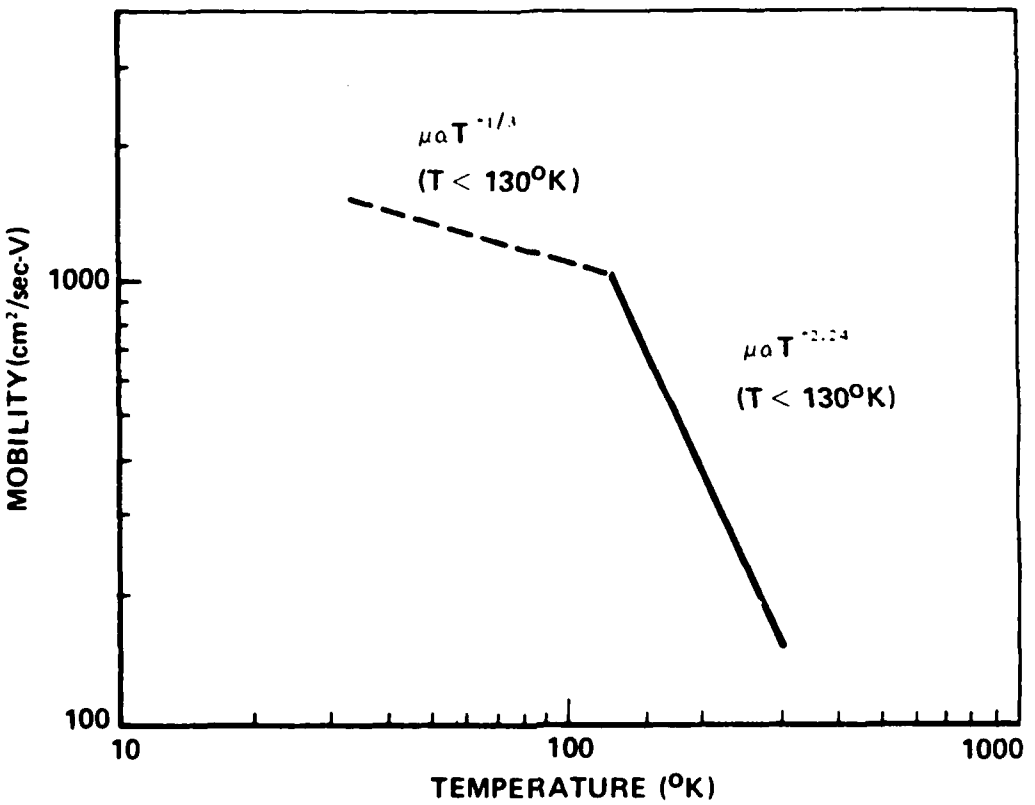

Figure 30b. Temperature dependence of mobility.

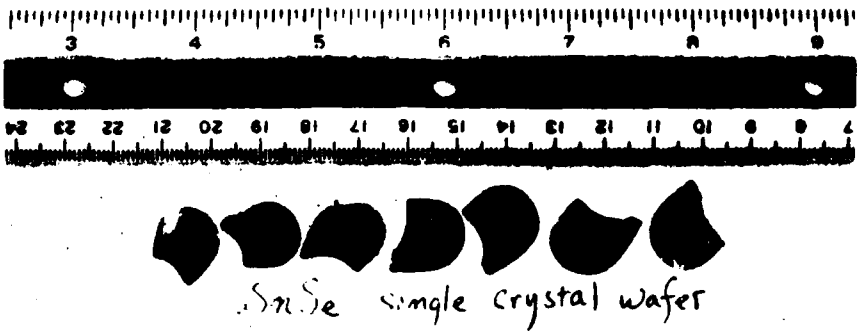

Figure 31. Thin wafers of SnSe used for Optical Measurement.

absorption edge, the absorption behaves [62] as

$$\alpha\ h\nu = A(h\nu - E_g \pm E_p)^n$$

where $h\nu$ is the photon energy, E_p is the phonon energy, and E_g is the electron energy at band gap. For direct transition (E_p=0), n is equal to 1/2 for allowed transitions and 3/2 for forbidden transitions. For indirect transitions, n is equal to 2 for allowed transitions and 3 for forbidden transitions. The square root of $\alpha\ h\nu$ is plotted against $h\nu$ for SnSe in Figure 34. The extrapolation of the curve to zero $(\alpha\ h\nu)^{1/2}$ yields an energy band gap of 0.924 eV. A simple interpretation of absorption transitions without considering the decomposition of multiple transition does give a value of energy band gap which compares favorably with a value from a photoresponse measurement of a SnSe diode. This agreement will be discussed later.

c. Interference Spectrum of Cleaved SnSe Layer and its Index of Reflection

One of the distinguishable characteristics of SnSe is that it can be easily cleaved along (001). Figure 35a shows cleaved layers of a SnSe single crystal. These layers were cleaved with a double-sided scotch tape with one side firmly pressed on a piece of glass slide. The thickness of the layer was determined using calibrated scanning electron microscopy. Figure 35b shows a SEM picture on the edge of a cleaved layer.

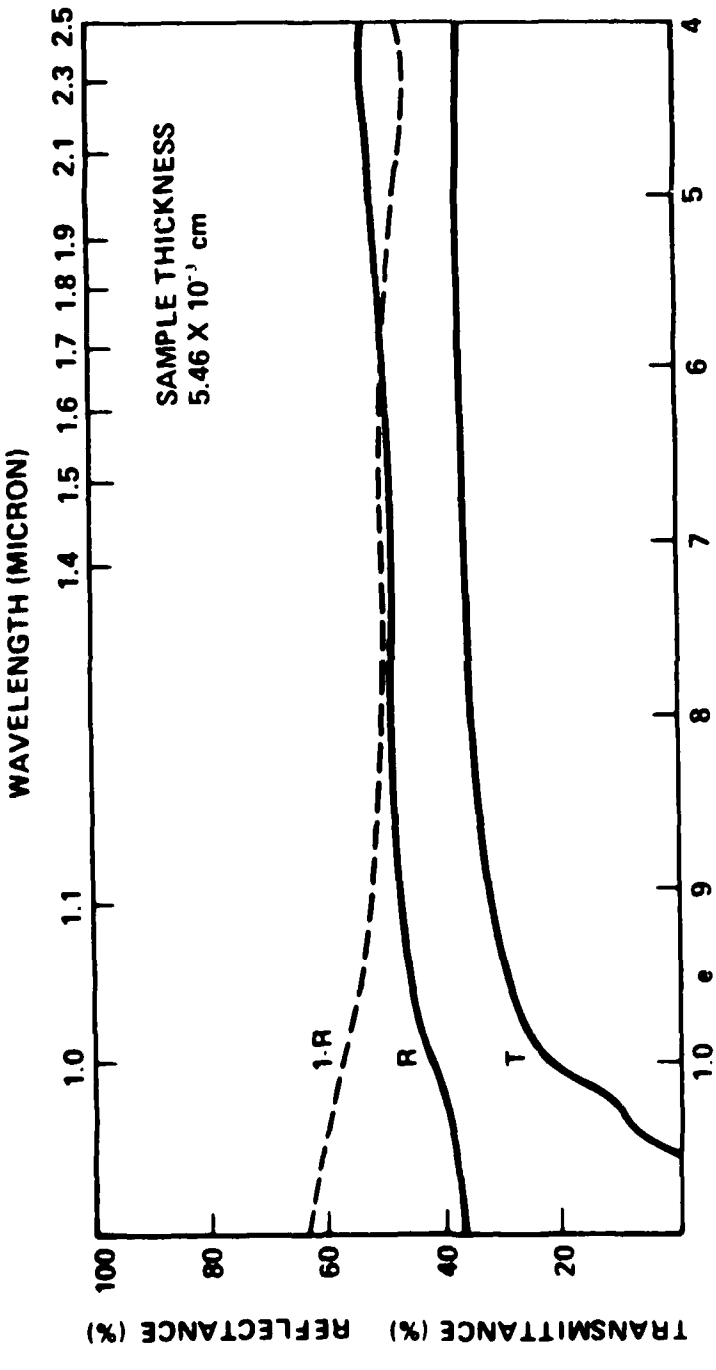

Fig. 32. Transmittance and reflectance of SnSe.

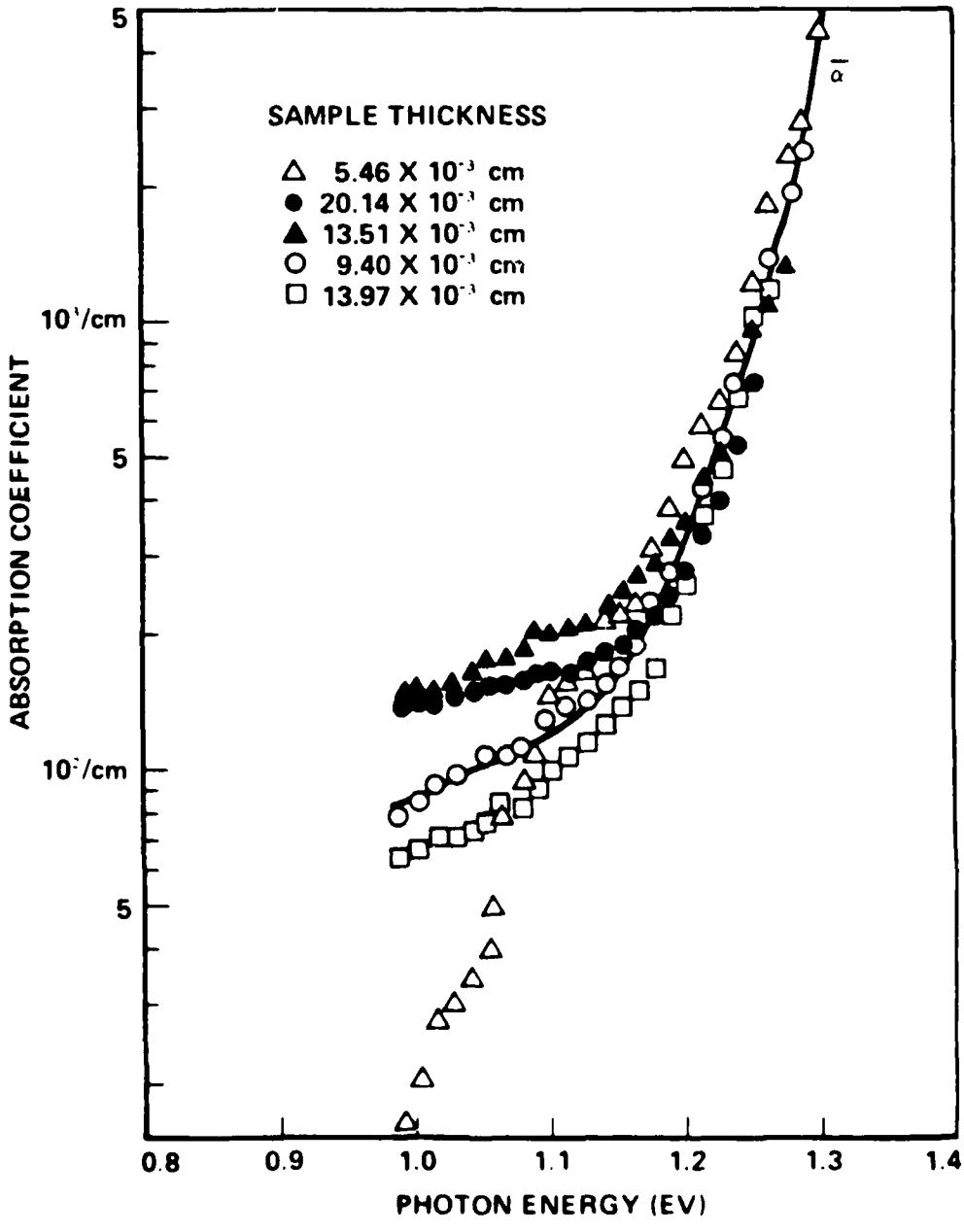

Fig. 33. Absorption spectra of SnSe

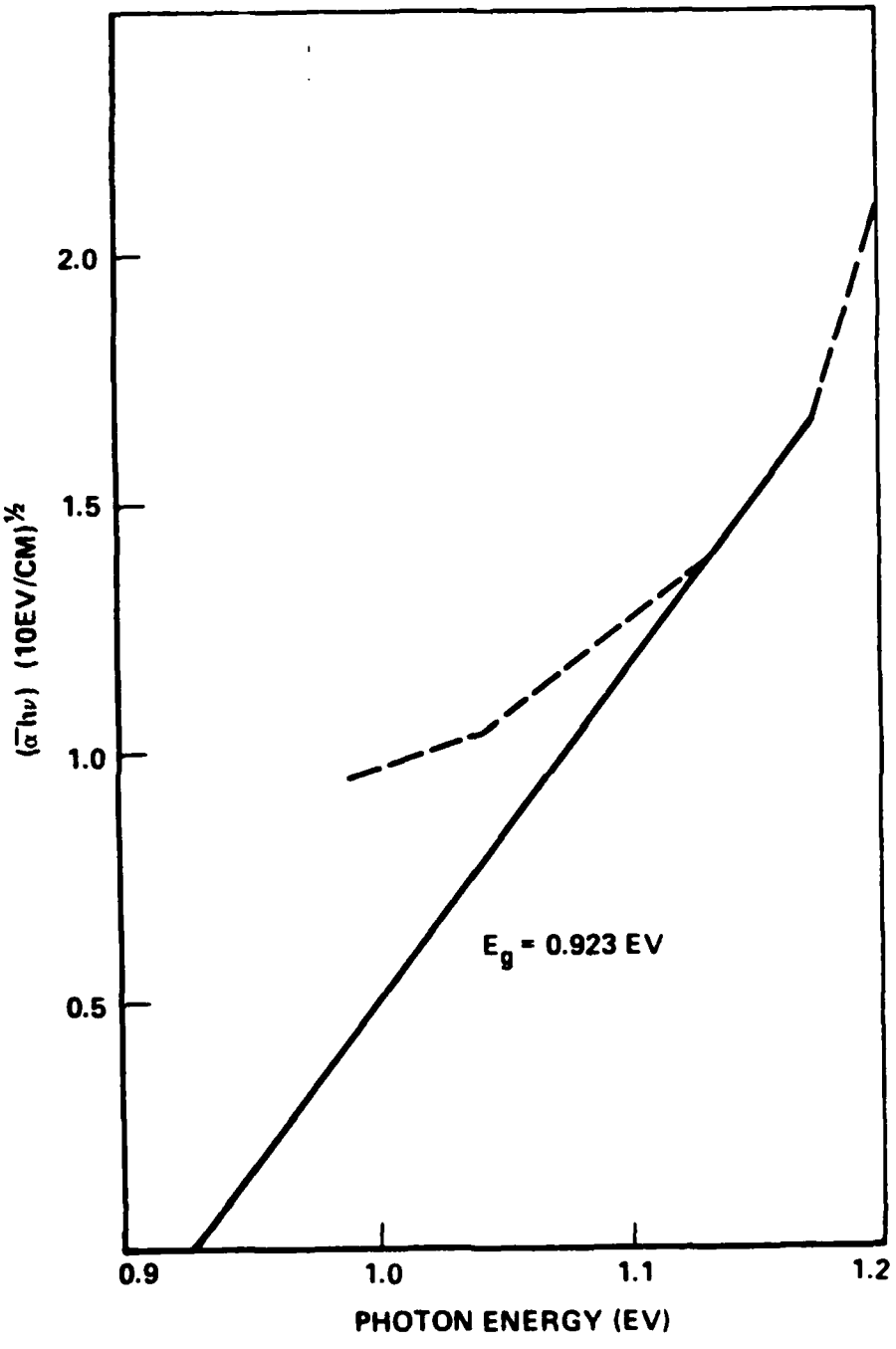

Fig. 34. $(\bar{\alpha}h\nu)^{1/2}$ vs $h\nu$.

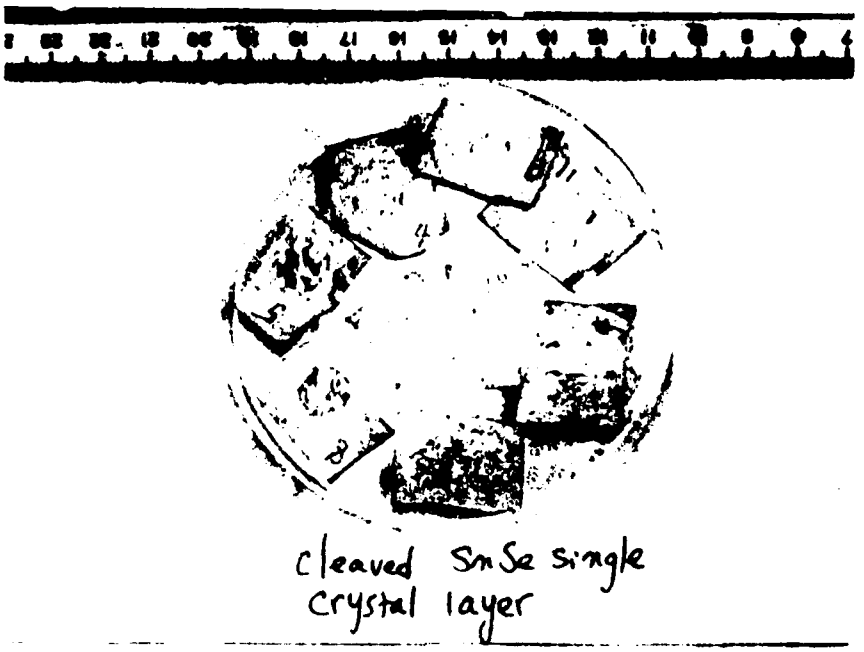

Cleaved SnSe single crystal layer

Figure 35a. Cleaved SnSe layers for interference measurement.

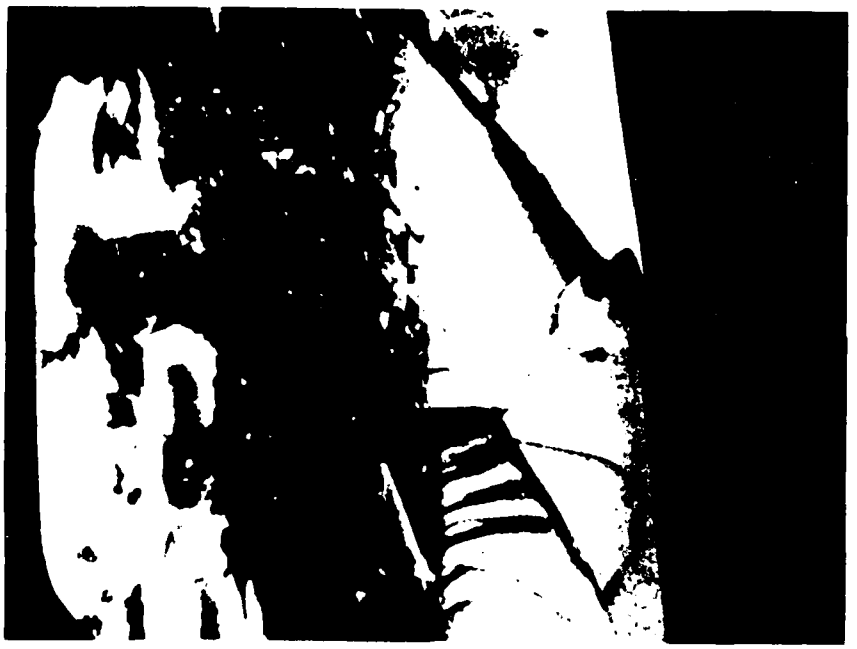

16.57μ

Figure 35b. SEM Picture of cleaved SnSe layer (16.57μ).

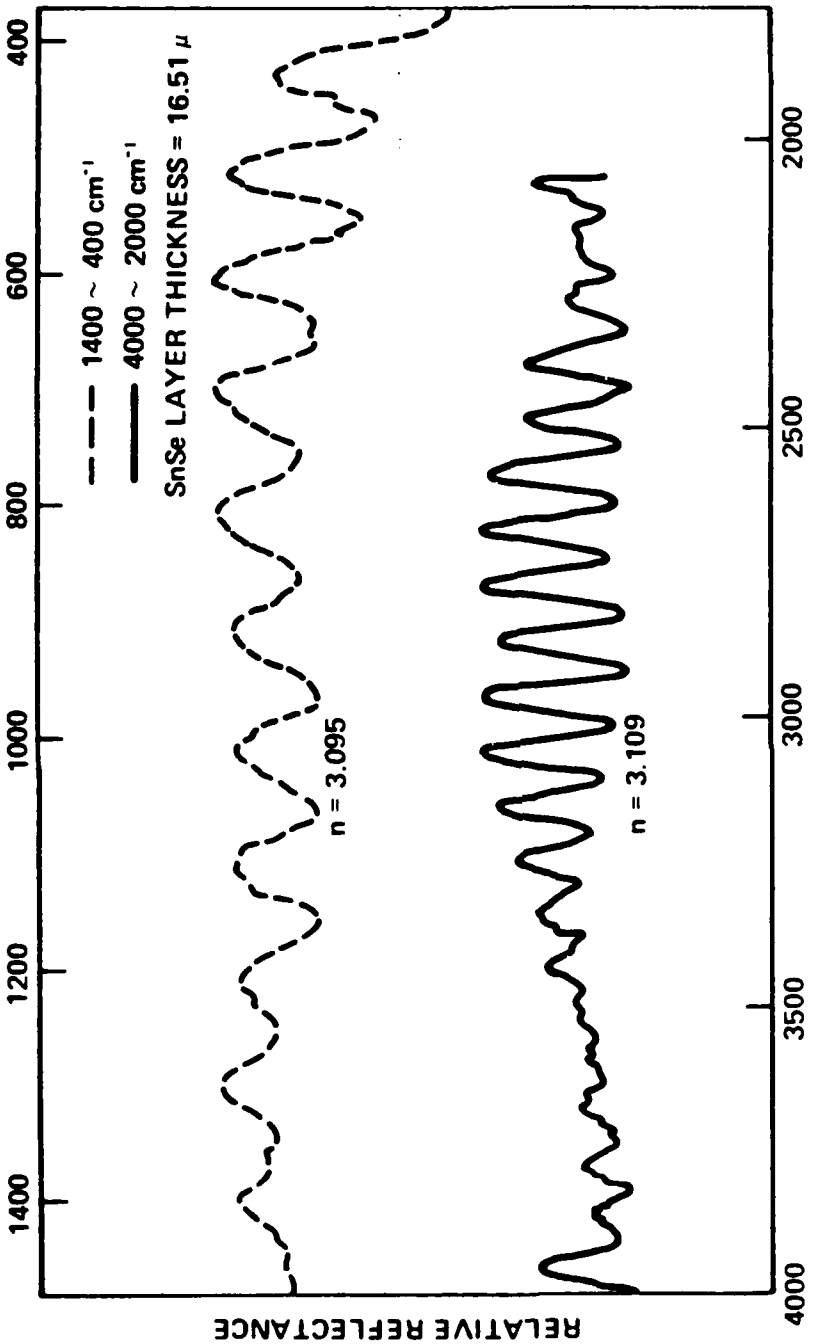

Fig. 36a. Reflection interference spectra of cleaved SnSe layer (16.51 μ).

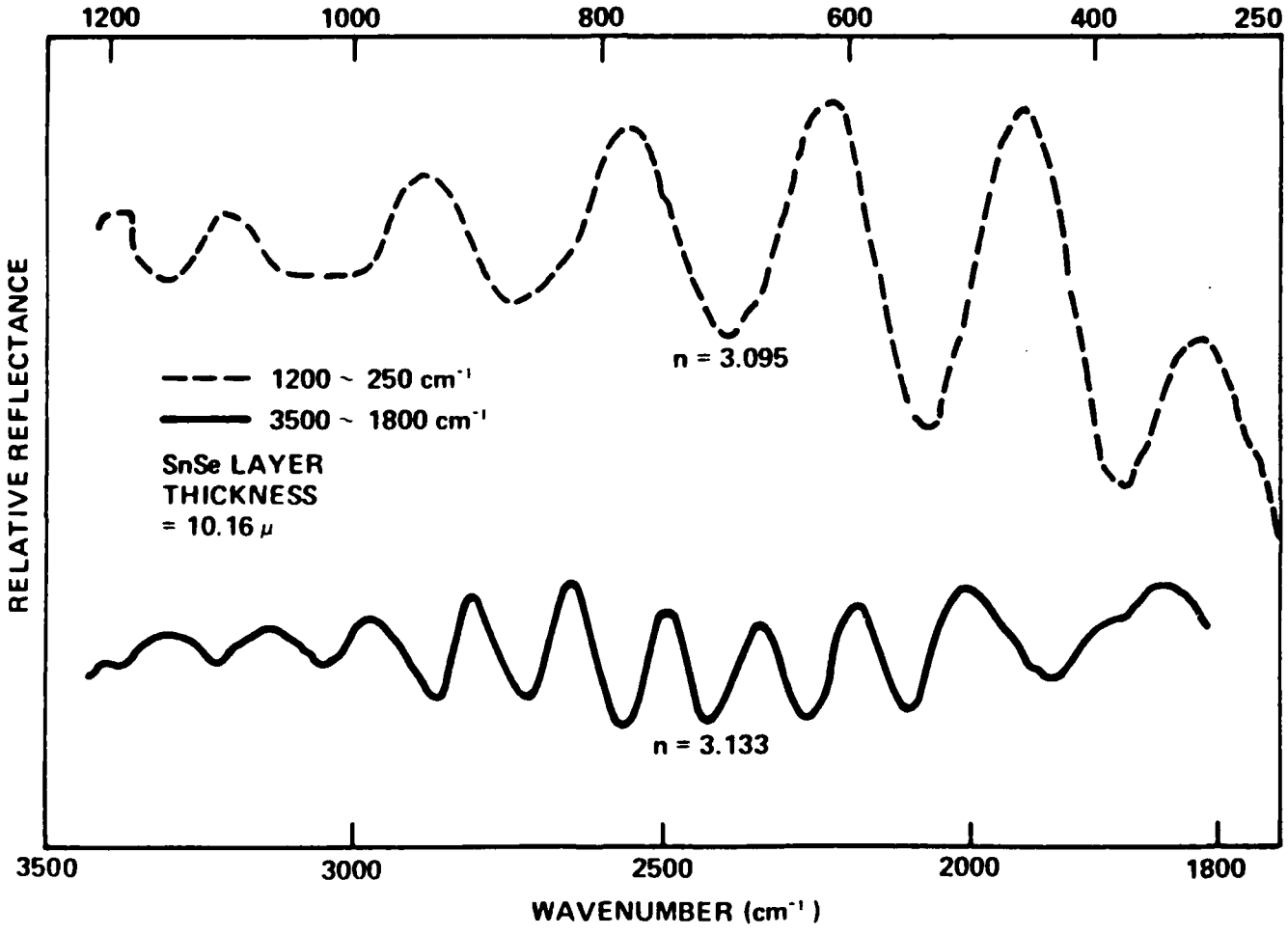

Fig. 36b. Reflection interference spectra of cleaved SnSe layer (10.16 μ).

Although layered samples were not perfectly flat, reasonably good reflection interference can be obtained from these samples. The reflectance was measured from 2.5 to 40 micrometers of wavelength using a Perkin-Elmer spectrophotometer, Model 457. Figures 36a and 36b show two of the interference spectra. The index of reflection n is determined using the following equation, $t = m/2(\mu_2-\mu_1)(n^2-\sin\theta)^{1/2}$ where μ_1, μ_2 are the peak frequencies (cm^{-1}), m is the number of fringes between μ_1 and μ_2, θ is the incident angle of 20° and t is the thickness in cm. The average value of the index of reflection is equal to 3.120 at 3 microns and 3.085 at 15 microns. Within this wavelength range, the band to band absorption can be neglected which gives a dielectric constant $\varepsilon_\infty = 9.6$.

E. SnSe P/N Junction

a. Diode Formation and I-V Characteristics

The as-grown SnSe single crystal has P-type conductivity which is caused by deviating the stoichiometric composition to the selenium side. Basically N-type SnSe can be formed with tri-valence elements, such as Al, Ga, In and Sb as dopants. Alternatively, it can be obtained by deviating the composition to the tin-rich side. An isothermal annealing of a P-type SnSe crystal in the presence of a solution of SnSe + Sn can achieve the purpose. The same result can also be achieved by diffusing Zn or Cd into the SnSe crystal. In this study, a simpler technique by alloying a tin film into SnSe

crystal is employed to produce a N-type SnSe crystal. In the close-tube-vapor-transport experiment, the crystal in ampoule A after sublimation (tin-doped) has a N-type surface due to a deficiency in selenium. Therefore, an as-grown P/N junction was readily obtained for the fabrication of a diode. Ohmic contacts were made by depositing dots of gold film on the N-side of the crystal. On the P side large area of tin film serves as an ohmic contact. The current-voltage characteristics were measured by applying an AC voltage of a sine wave to the diode in series with a variable resistor which limits the current. The voltage across the resistor was fed to the X-axis of an oscilloscope (Tektronix, model 503) as the current signal. The voltage across the diode was fed to the Y-axis as the voltage signal. The I-V curve of the as-grown P/N diode is shown in Figure 37. The forward bias gives a fair injection whose cause is suspected to be due to a high contact resistance between the ohmic contact pad and the point needle. In a further study, a silver epoxy was used for bonding the gold wire to the ohmic contact pad. A thin tin film was deposited [illegible] etched P-type SnSe substrate at a vacuum of 10^{-6} Torr. The thickness was measured to be around 2000 Å with an interference [illegible]. The sandwich was annealed at 480°C for two hours [illegible] Torr. Hot probe method subsequently confirmed [illegible] was formed. The film started to melt around 237°C, [illegible] visual during annealing. Although tiny tin drops [illegible] were formed on the surface, the N-type surface

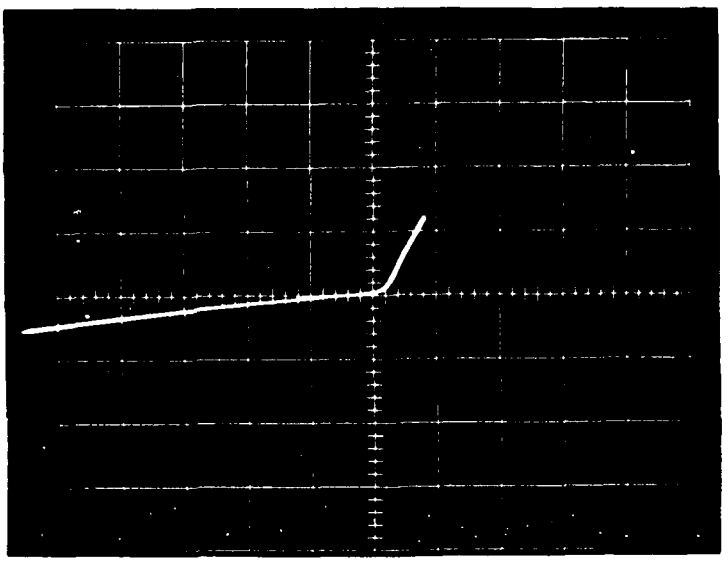

Figure 37. I-V of as-grown P-N junction (IOmA/div., I V/div.)

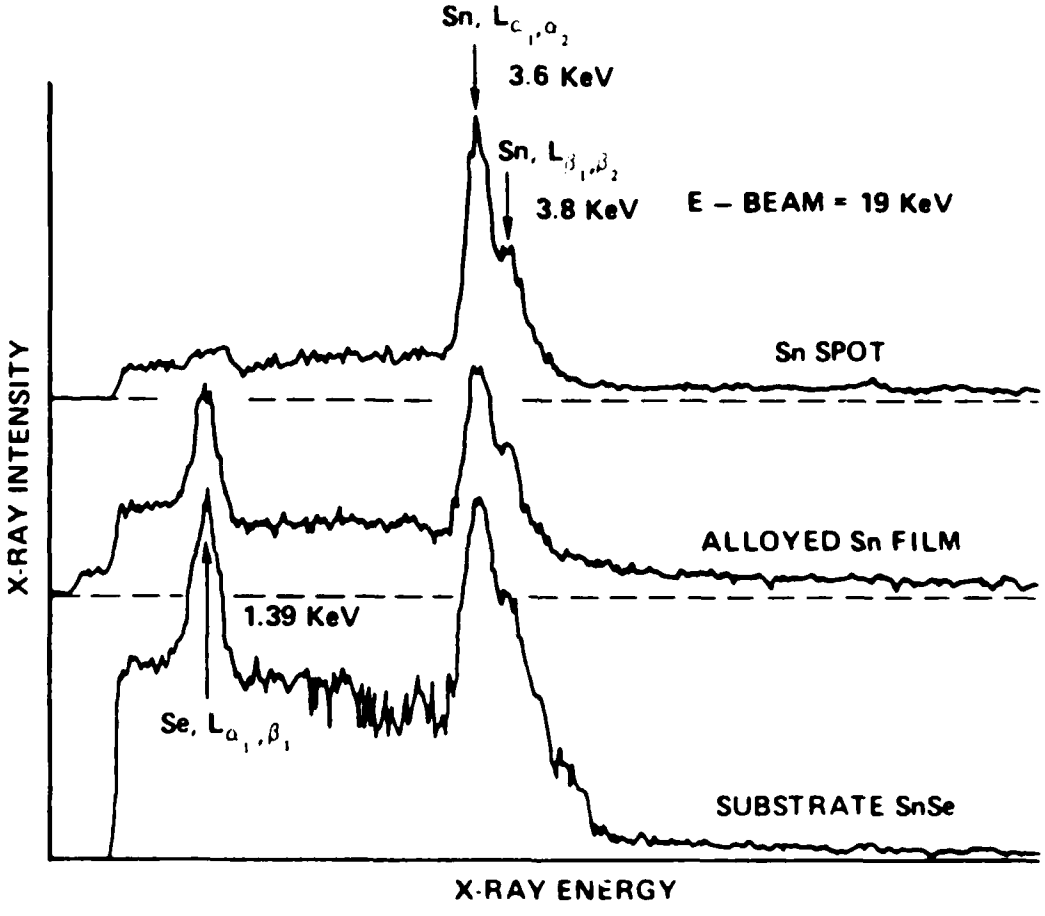

Fig. 38. X-RAY spectrum of alloyed SnSe diode

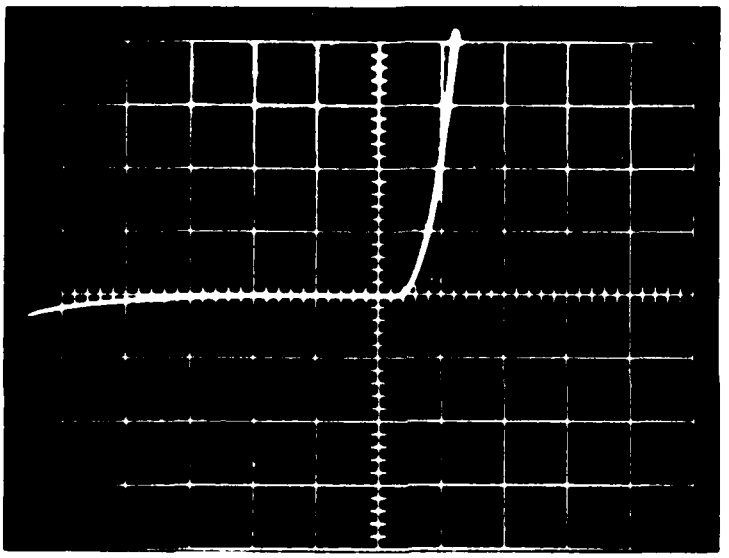

Figure 39 I-V of point contact on alloyed P film of SnSe (1 mA/div., 1 V/div.)

was preserved without showing any metallic conduction. Figure 38 shows a microprobe examination of the alloyed SnSe diode which contains tin drops on its surface. When the annealing temperature was below 300°C, the tin films were converted to a P-type surface instead of a N-type. The I-V curve of a Pb/Sn solder point contact on the converted P-type surface is shown in Figure 39. Its large break-down voltage (compared with the substrate) indicates that the P-surface has a much lower hole concentration than the substrate. After exposing the P-surface for three days in air, the I-V curve started to show a switching phenomenon which is shown in Figure 40a. After the breakdown, the switching phenomenon disappeared, as shown in Figure 40b. The switching effect was also observed on a bulk SnSe crystal. Figure 41 shows the I-V curve of two points in contact with the surface of the crystal. A noticeably large negative resistance exists after the breakdown. The alloyed SnSe diode also exhibits a negative resistance after the breakdown at 3 volts as shown in Figures 42a and 42b. The diode has a In film dot on the N side and a large tin film on the P-side serving as the ohmic contact pads. Gold wires were bonded to the pads by applying a silver epoxy as an adhesive. The I-V curves of the alloyed SnSe diodes for small forward bias were measured on a Tektronix curve tracer,Model 557. One result is shown in Figure 43. An average n value of 2.08 was figured out for fitting the equation of $I = I_o e^{qv/nKT}$, where q is the electronic charge, K is the

Boltzmann's constant, V is the voltage and T is the absolute temperature. The n value of 2.08 indicates a dominant surface recombination existing in the alloyed diode. The measurement of capacitance versus voltage was not successful due to a large leakage current in the diode. Further studies on a smaller junction-area diode were not pursued. However, the relative carrier concentration versus depletion depth plot was measured on the I-V plotter made by Materials Development Corporation, Santa Monica, CA.

Two of the curves are shown in Figures 44a and 44b. Since the junction area and the static dielectric constant were not available, a detailed analysis was not pursued. But to the first order, the behavior of a grade junction can be observed in Figures 44a and 44b. During alloying, the melt tin film dissolved a small amount of SnSe according to a solid solubility curve at the alloying temperature. And since this melt was not in thermodynamic equilibrium with the substrate, a subsequent diffusion between the liquid and the solid followed such that a non-step junction was formed. The cooling of the melt really did not affect the diode formation. However, tin drops might have been formed during the diffusion process.

Attempts have been made to produce a thicker tin film and to anneal at a shorter time. In both cases, larger drops of tin metal was formed on the surface of the diode. Diodes made this way tended to show a larger leakage current.

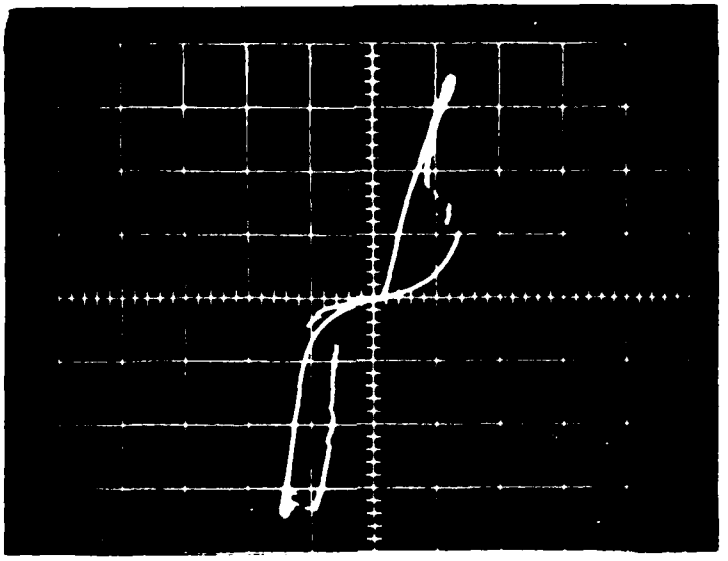

d

Figure 40a. I-V of point contact on degraded alloyed SnSe film (p-type) (2mA/div., I V/div.)

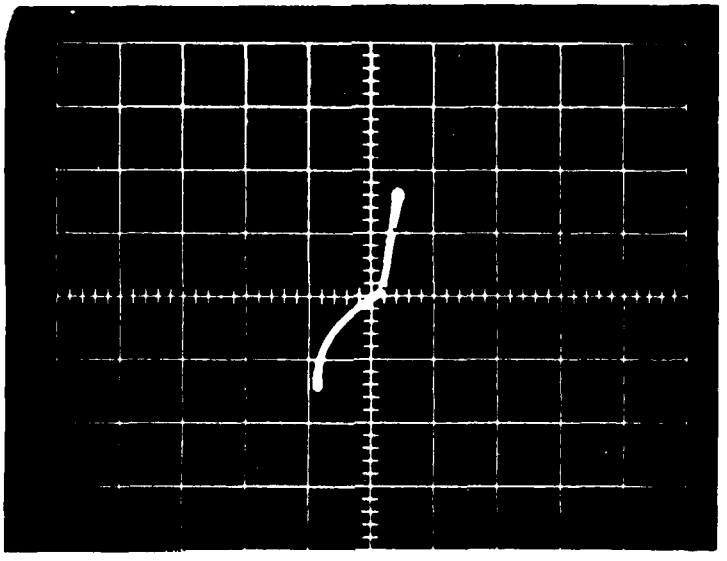

e

Figure 40b. I-V of point contact on degraded P-type film of SnSe after breakdown. (2 mA/div., I V/div.)

Figure 41 I-V Curve of two point contacts on SnSe crystal.

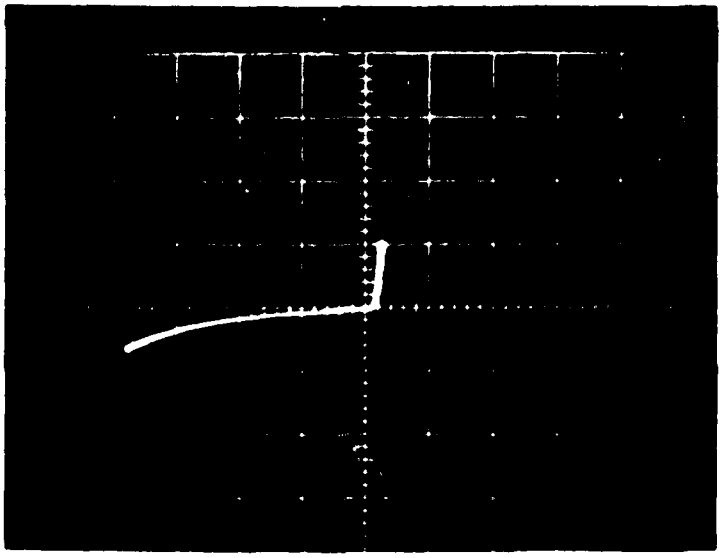

Figure 42a. I V curve of alloyed P N junction of SnSe (10mA/div., I V/div.)

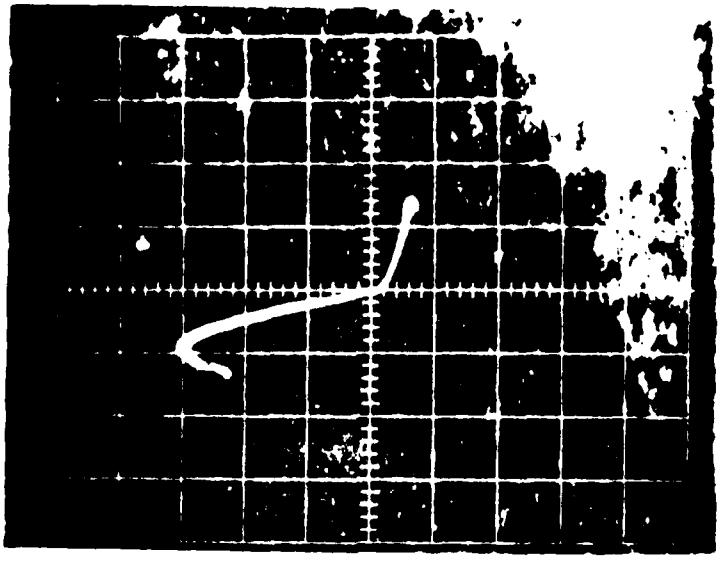

Figure 42b. Negative resistance of SnSe diode (10 mA/div, 1 v/div).

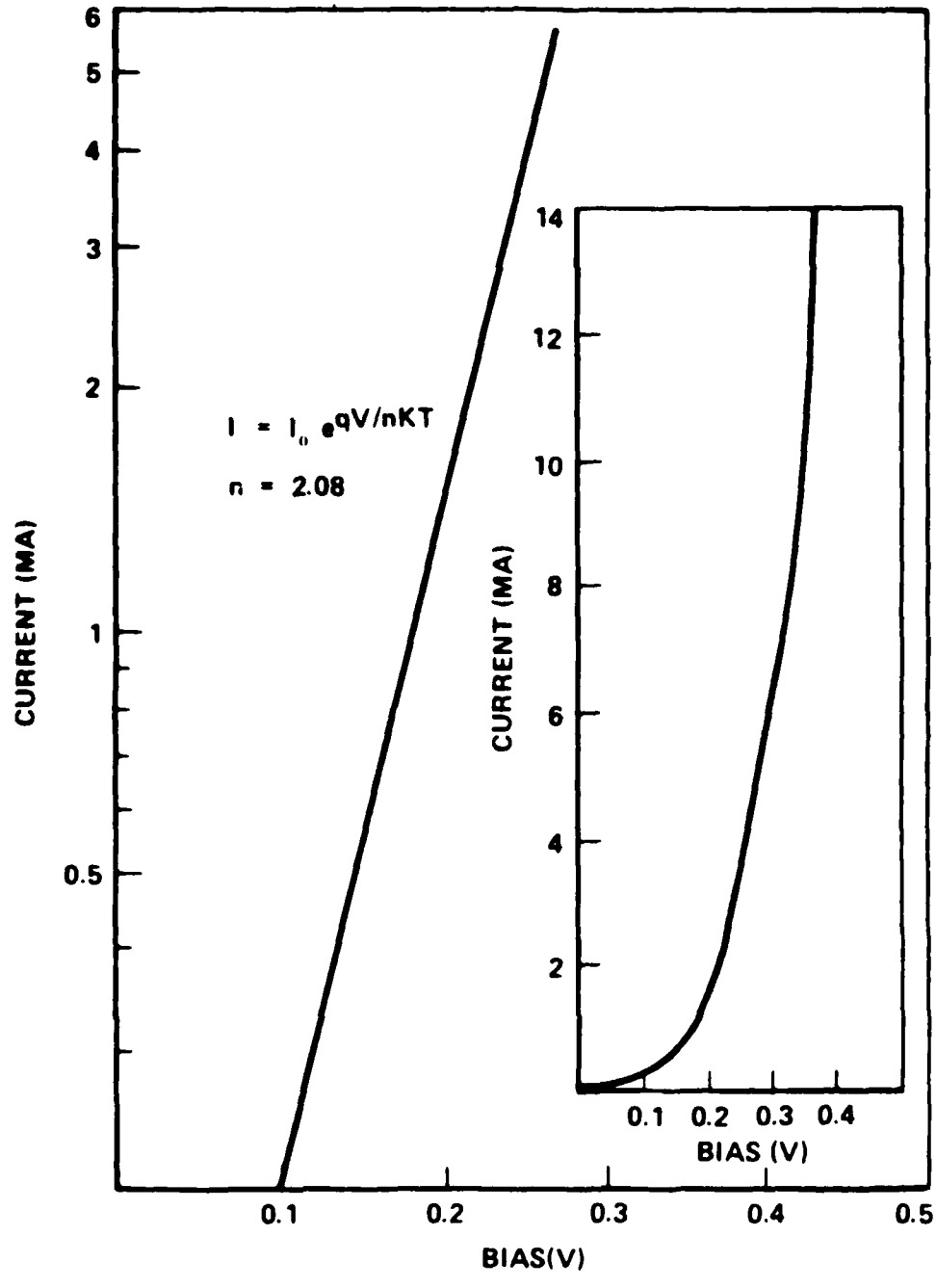

Figure 43. I-V curve of SnSe diode (n = 2.08 for forward bias).

b. Photoresponse and Electronic Energy Band Gap

The photoresponse was measured on one of the diodes over a range of wavelengths from 0.84 to 1.31 micrometers. A 3-ohm resistor was connected to the diode and the voltage across the resistor was recorded as a function of wavelength. In this experiment, the light source from a G.E. tungsten light bulb (500 W) was first passed through an IR-pass filter, entered the entrance slit of a Baush & Lomb monochrometer and focused on the diode. Since the distribution of spectrum was unknown, an Epply thermopile with a quartz window was used to calibrate the light intensity. To make sure that the data were correct, a Tektronix digital photometer with a J 6502 probe was used to check the intensity at 0.85 micron wavelength. After normalizing the photoresponse which presents the response to a uniform spectrum, the photoresponse was normalized again to give a 100% response at its peak response. The result is shown in Figure 45. The diode produced 24.4×10^{-6} volts at 1 micrometer wavelength of 4.65 mw/cm^2. Although a cut-off photon energy of 0.942 eV is read from Figure 45, it does not represent the energy band gap of the SnSe. If we assume that the short circuit current of the diode is proportional to the absorption coefficient, a plot of $(\alpha_h h\nu)^{1/2}$ versus photon energy ($h\nu$) is given in Figure 46, which yields the energy band gap value of 0.922 eV by extrapolation. The other values, 0.925 and 0.943 eV, might be the band gap energy for the other $\vec{k}$ directions because SnSe has an orthorhombic crystal structure.

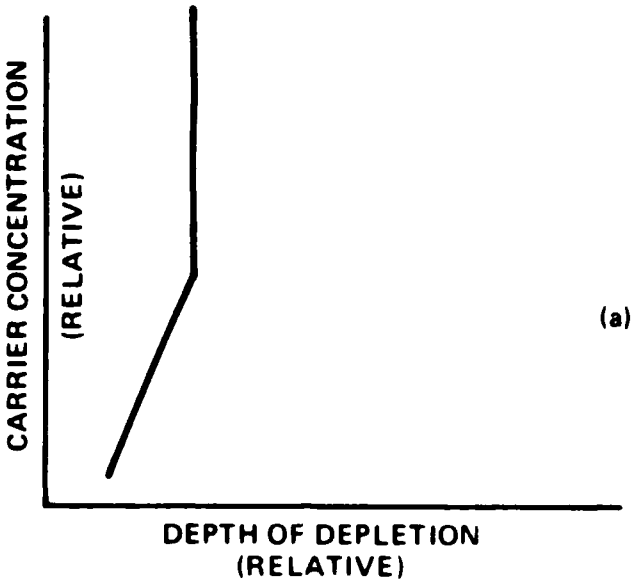

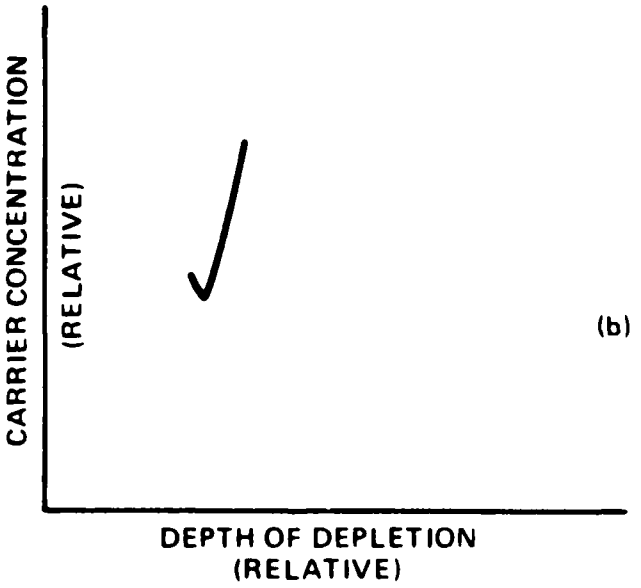

Fig. 44a and 44b. Relative doping profile of alloyed P/N junction of SnSe

F. Preparation of SnSe Film

a. Close-Space-Vapor-Transport

The close-space-vapor-transport technique, described in Section 3C, was used to deposit a SnSe film on $SnSe_2$ and SnSe substrates. Preliminary studies show that SnSe starts to sublime substantially at 440°C and at a vacuum of 10^{-6} Torr. Therefore, the close-space-vapor-transport technique was used to evaporate a SnSe source to a SnSe substrate, at a source temperature of 440°C and the substrate temperature of 176°C with a separating distance of 1.5 cm. Only P-type SnSe film could be obtained. The SnSe film deposited on $SnSe_2$ substrate did not show a good adhesion, probably due to a large lattice mismatch between the film and the substrate. Polycrystalline SnSe film was obtained due to a lower substrate temperature. Figure 47 shows a SEM microphotograph of a polycrystalline SnSe film. Its composition as shown in Figure 48 was checked by microprobe analysis and found to be the same as the substrate.

b. Liquid Phase Epitaxial Growth

The LPE growth of a SnSe film on a SnSe substrate was performed using a vertical dipping technique. Owing to the sublimation of the melt at 500°C, the substrate was covered with contamination before it went into the melt, resulting in an island growth. Therefore, a tilting technique was adopted for subsequent LPE growth. A boron nitride crucible, shown in Figure 49, was machined and placed on the top of a graphite heater. The crucible has two interconnected cells acting as containers for the melt and the substrate. A gyroscope-

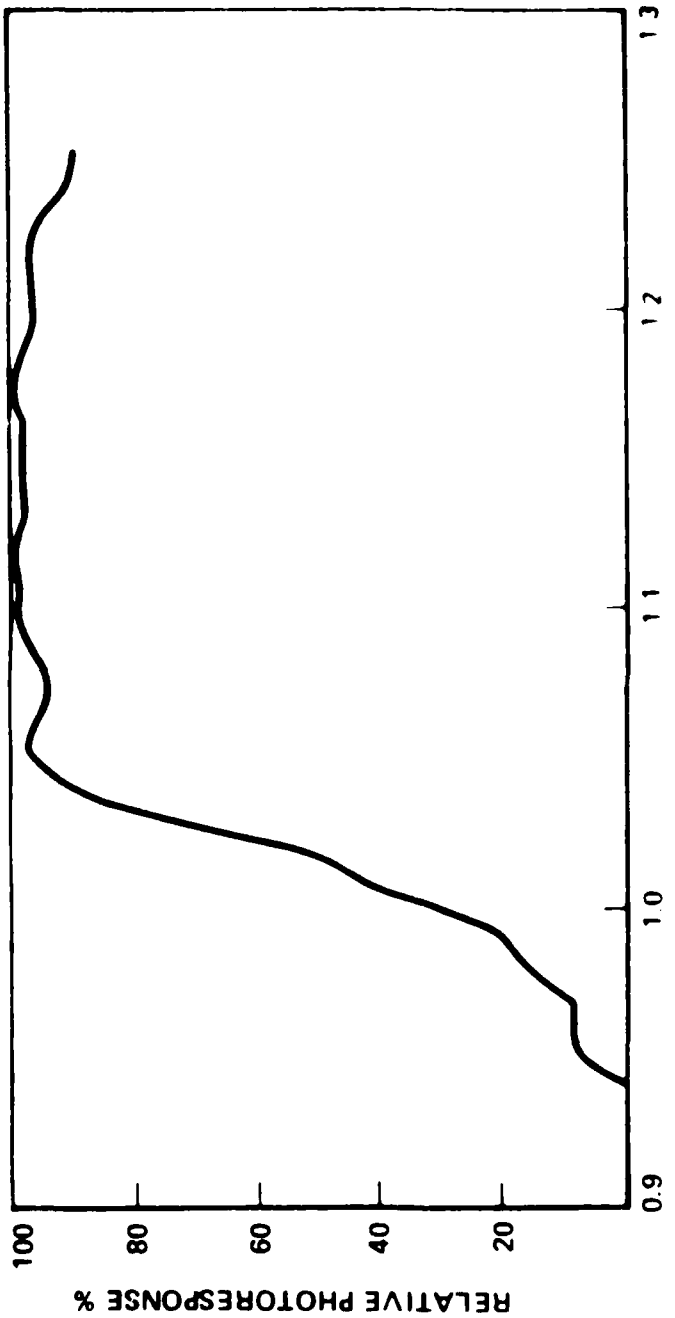

Figure 45 Photoresponse spectra of SnSe diode

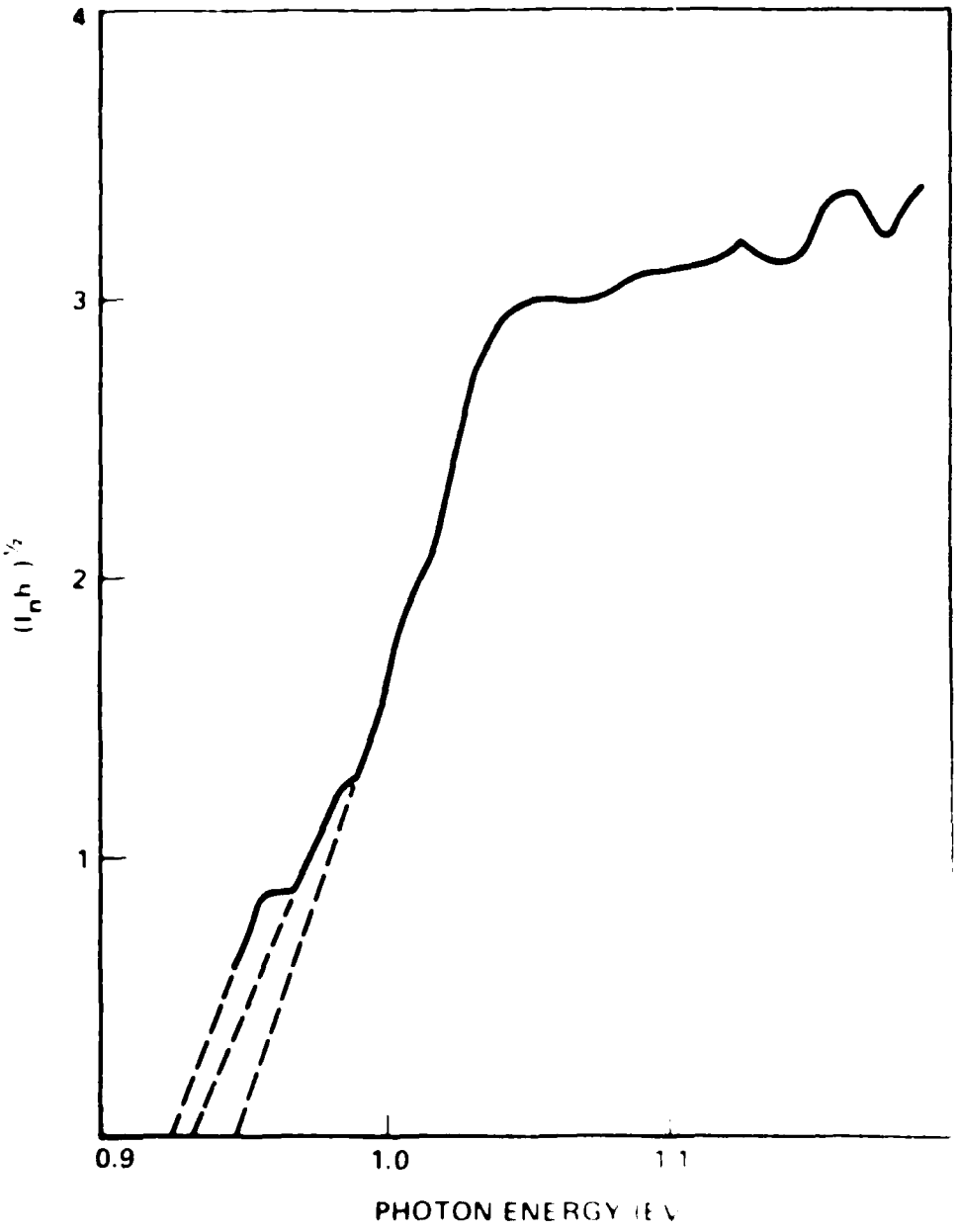

Fig 46 $(I_n h\nu)^{1/2}$ vs $h\nu$ of SnSe direct

AD-A179 773 SEMICONDUCTOR EUTECTIC SOLAR CELL(U) CALIFORNIA UNIV 2/2
LOS ANGELES SCHOOL OF ENGINEERING AND APPLIED SCIENCE
A S YUE ET AL. DEC 86 UCLA-ENG-8808 RADC-TR-86-170
UNCLASSIFIED F19628-77-C-0021 F/G 20/12 NL

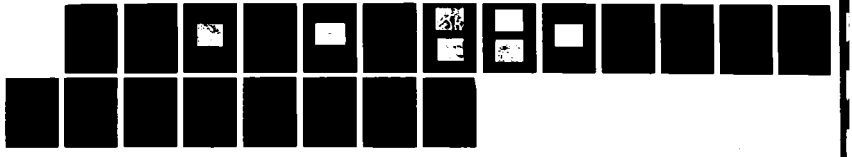

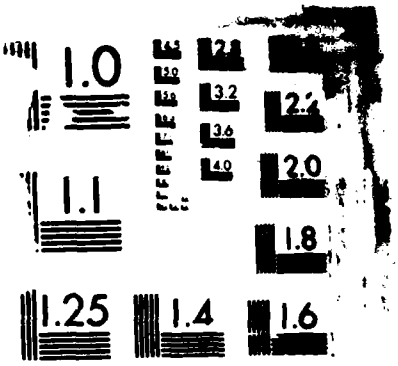
1.0
1.1
1.25
1.4
1.6
2.8
3.2
3.6
4.0
2.2
2.0
1.8

type frame was designed to provide the crucible with a leveled tilting movement. Two thermocouples were used to control and monitor the temperature of the melt. The operation was performed inside a vacuum chamber at 10^{-6} Torr. Due to heat loss, a steep temperature gradient was present in the melt. Accordingly, it was necessary to obtain large oversaturation in the melt to allow the epitaxial growth to take place on the substrate. The explanation is given in Figure 50. An oversaturated melt would be able to have the equilibrium and actual temperature profiles to be arranged such that the nucleation process could start on the substrate. Melting back of the substrate occurs if the solution is not oversaturated. Figure 51 shows the microstructure of the melt-back of the SnSe substrate. Droplets of Sn usually were trapped in the substrate due to its terrace structure. Figure 52 shows the LPE SnSe film grown on the SnSe substrate. The procedure for growing this film is as follows: the tin melt was saturated with SnSe at 457°C for two hours and slowly cooled to 433°C, this oversaturated melt was then tilted over the substrate and cooled to 389°C in 50 minutes; the growth was stopped by tilting the melt from the substrate to the other cell. A small amount of tin melt was left over and still can be seen from Figure 52. The surface of the LPE grown SnSe film exhibits feature-like morphology which is shown in Figures 53 and 54. The array of the feature structure is suspected to be related to the constitutional supercooling which causes the breakdown of the solid-liquid interface. The shape of the interface is

Figure 47. Close-spaced-transport Polycrystalline of SnSe (X 2700).

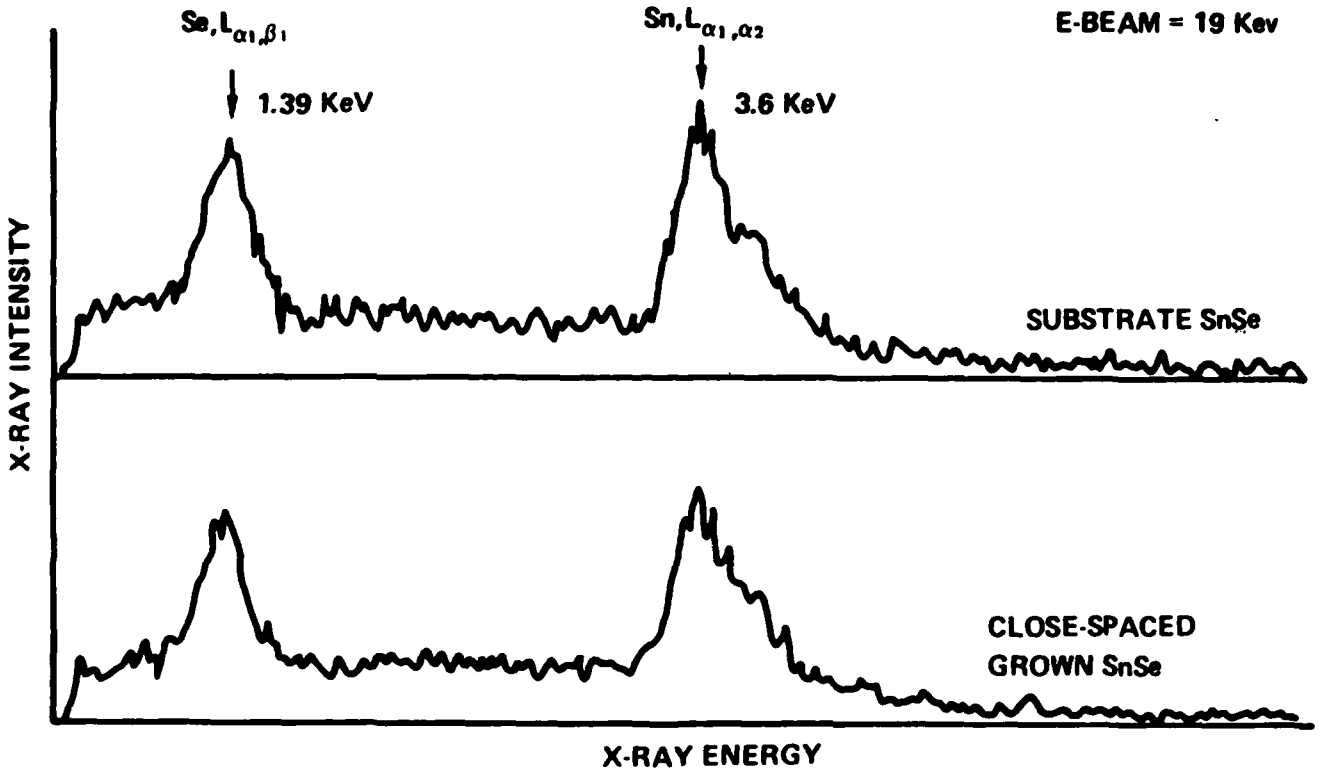

Figure 48. X-ray spectrum of close-spaced-grown SnSe.

Figure 49. An apparatus of LPE growth of SnSe in vacuum.

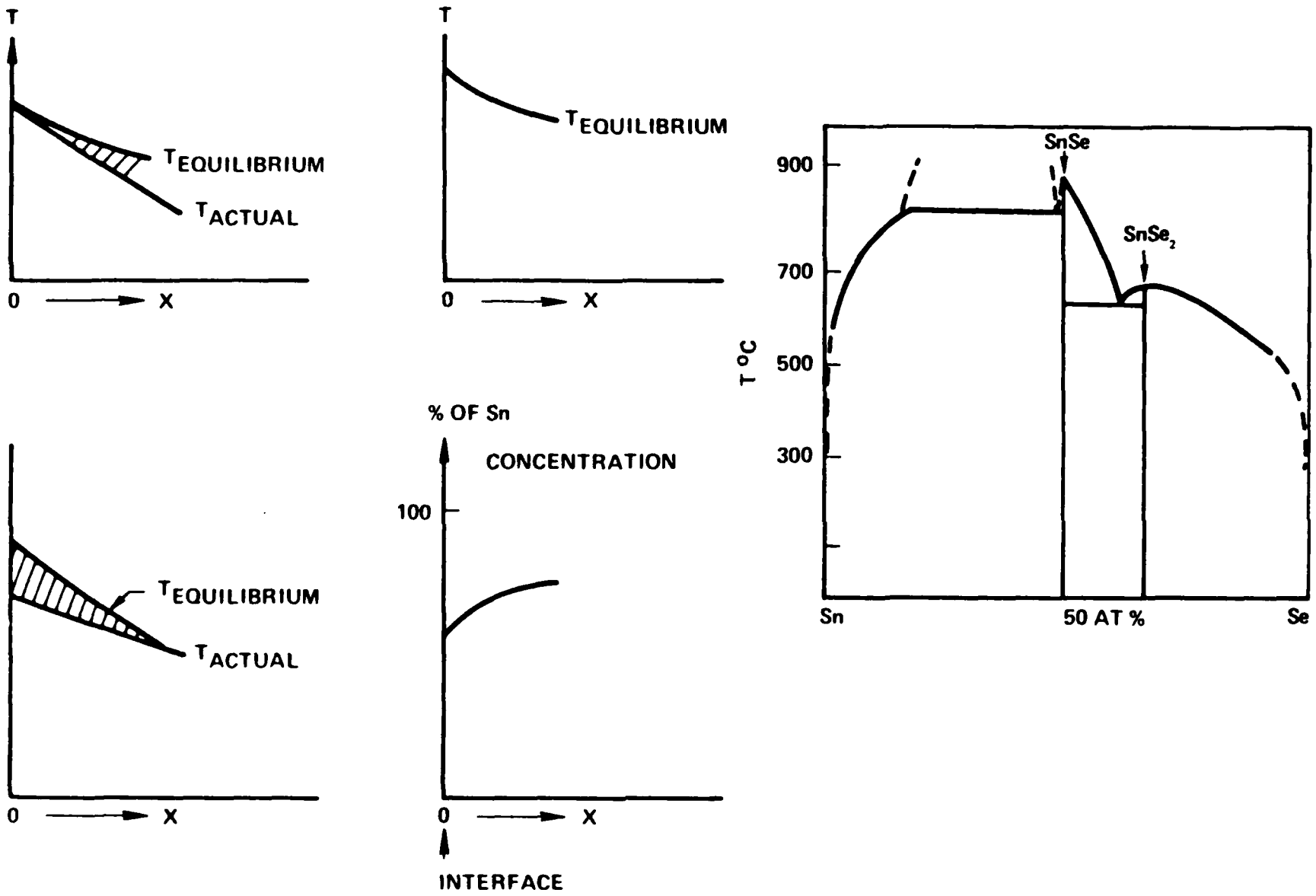

Fig. 50. Explanation of oversaturation of SnSe in LPE experiment.

4μ

Figure 51. SEM Picture of etched back Substrate of SnSe

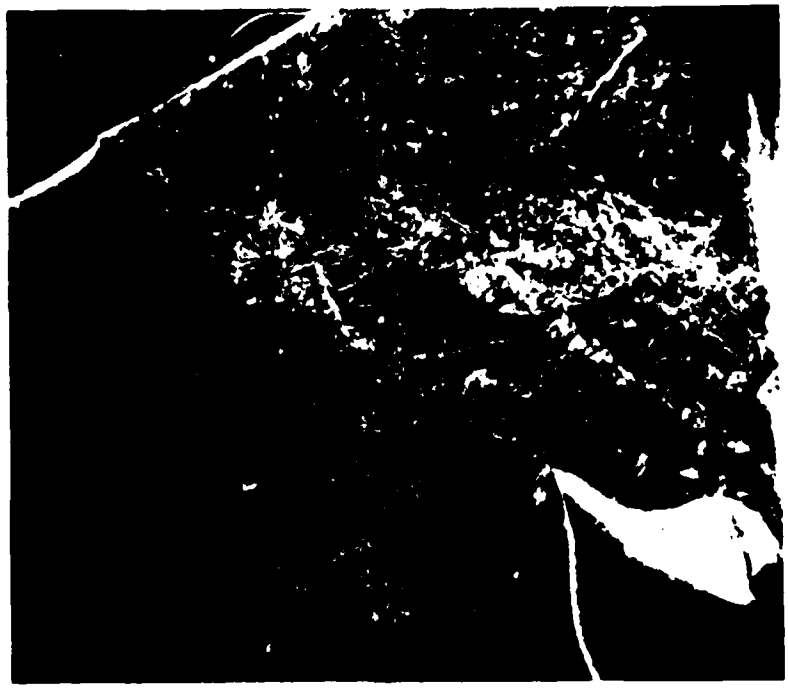

Figure 52 SEM Picture of LPE film of SnSe (X35)

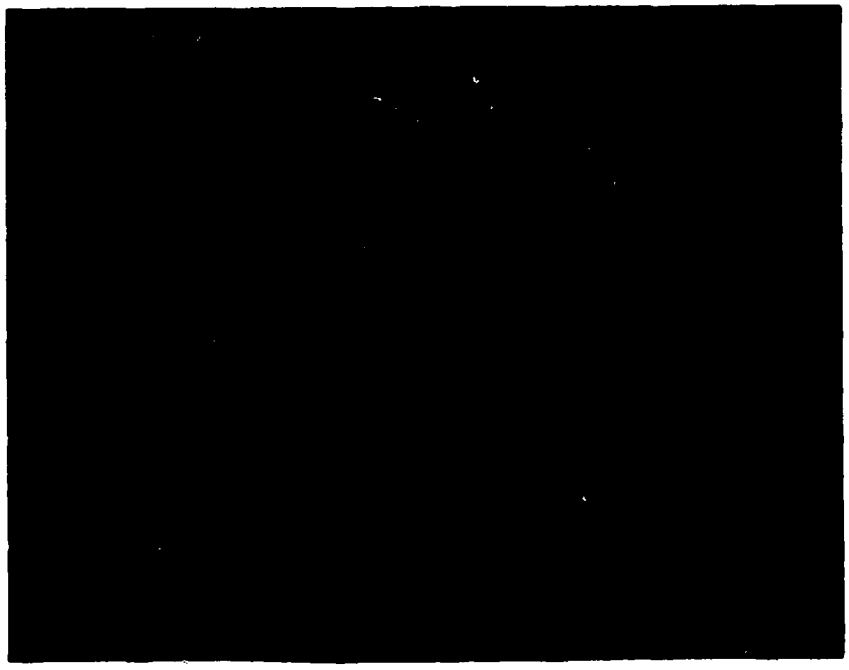

20μ

Figure 53. SEM Picture of feather-like surface morphology of LPE film of SnSe.

20μ

Figure 54. SEM Picture of valleys of feather array of LPE film of SnSe.

20μ

Figure 55. SEM Picture of surface morphology of LPE film of SnSe.

presumably related to the geometrical boundary condition. Because of the stress induced in the clamped substrate, kinks were produced on the surface of the substrate. It can be seen from Figure 55 that the values of the feature array run perpendicular to the curved islands. It is suspected that low valleys of solid-liquid interface is related directly to the valleys of the feature array. This feature-like morphology mainly displays on the surface near the edge of the film. However, the central portion of the film is spectacularly smooth. The lectron beam microanalysis was performed on the film. The result shown in Figure 56 indicates a uniform composition of the LPE grown film.

In principle, the film grown from the Sn-rich solution should have shown N-type conductivity, but P-type film of SnSe was obtained in this experiment. It is believed that either impurity in the melt or residue impurities in the crucible is responsible for the formation of P-type conductivity.

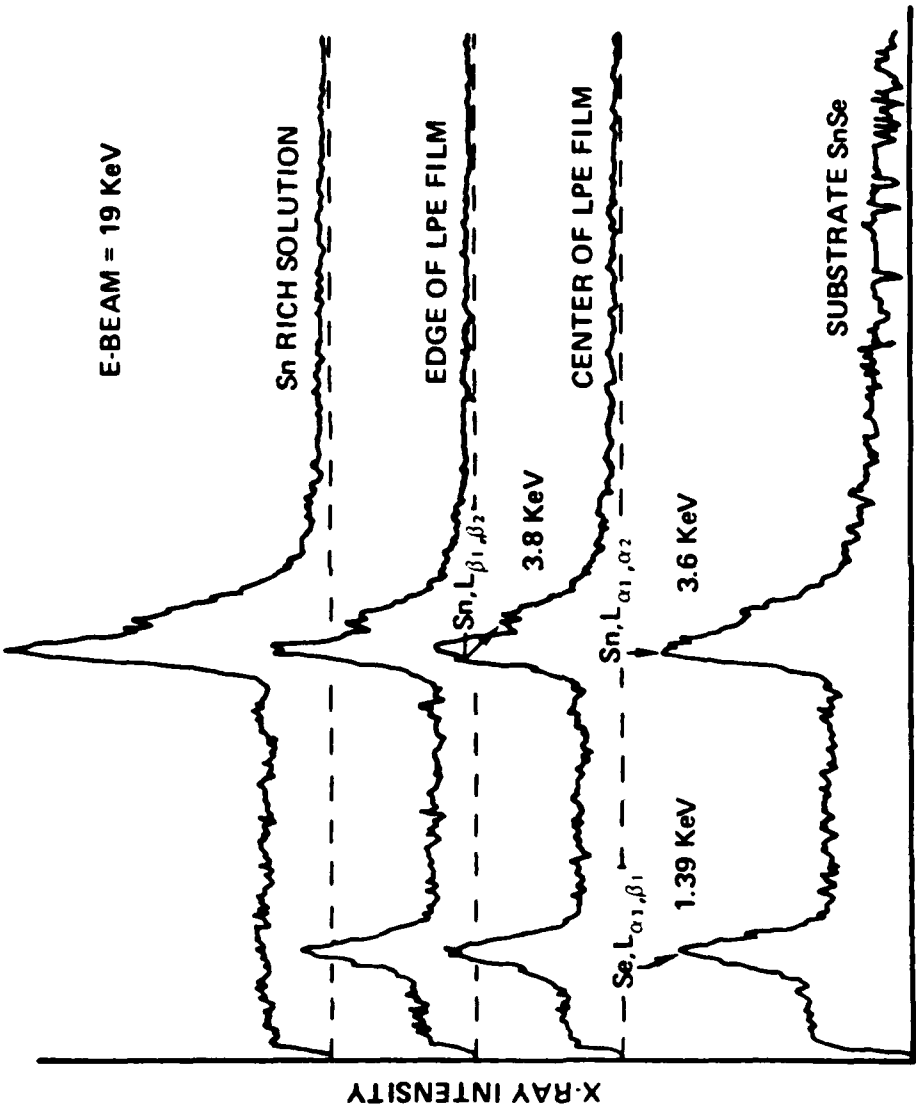

Figure 56. X-ray spectrum of LPE grown SnSe.

SECTION 5

SUMMARY AND CONCLUSION

Motivated by searching for an applicable semiconductor eutectics quasibinary semiconducting eutectic systems were searched and listed in this study. A binary SnSe-$SnSe_2$ eutectic was chosen as the topic for studies, based on its simplicity.

Bulk crystals of SnSe-$SnSe_2$ eutectic and $SnSe_2$ compound have been successfully grown using the Bridgman technique. A temperature gradient of 110°C/cm and a growth rate of 0.5 cm/hr were used for the growth. The multi-p/n junction characteristics of the SnSe-$SnSe_2$ eutectic was determined by measuring the cleaved layers of the eutectic with a hot probe. Further examination of the reflectance data in the infrared region shows a nondegeneracy of the eutectic. Films of SnSe and $SnSe_2$ have been prepared by means of a close-space-vapor-transport technique but they are not of high quality.

LPE growth of a SnSe film on a SnSe substrate has been successfully prepared at 433°C by the tilting technique. This LPE growth film shows a feature-like surface morphology near the edge.

By carefully selecting a supercooling (ΔT = 30°C), bulk single crystals of SnSe have been grown from the vapor phase at 800°C in a closed ampoule. Molecular vapor-transport is believed to be the mechanism for growing these single crystals. If the transport-temperature is below the eutectic temperature, $SnSe_2$ crystal can be grown

from a Se-rich charge. This is mainly due to a thermodynamic equilibrium between vapor species of SnSe and $SnSe_2$ at temperatures below the eutectic temperature. All the grown crystals are very soft. The cutting and polishing techniques applied to the processing of PbSnTe [63] were adopted for preparing the wafers. A chemical etching solution was developed, the oxidized surface shows interference colors whose sequence follow that of SiO_2 film on silicon [64]. For SnSe crystal, the optical absorption coefficient was measured near the band edge. The interference spectrum of reflectance measurements yields a value of 3.12 as the index of reflection of 3 micrometer wavelength and 3.095 at 15 micrometer wavelength. The extrapolation of the curve of $(\alpha\ h\nu)^{1/2}$ versus $h\nu$ yields an energy band gap value of 0.923 eV for the SnSe compound.

A SnSe diode made by alloying tin film of 2000 Å at 480°C for 2 hours in vacuum has a n value of 2.08 in the current-voltage equation, $I = I_o e^{qv/nKT}$, indicating that a surface recombination mechanism is prevailing. From the photoresponse measurement of the alloyed SnSe diode, curve of $(I\ h\nu)^{1/2}$ versus $h\nu$ was obtained. This curve indicates an electronic band gap of 0.922 eV. In conclusion, SnSe, $SnSe_2$ and SnSe-$SnSe_2$ eutectic are soft semiconducting compounds and mixture whose technological applications are restricted by the difficulties involved in materials processing and handling.

Although preparation of films of SnSe and $SnSe_2$ were successful as demonstrated in this study, the major inhibitions of applying

these techniques for liquid-phase-epitaxial growth of a SnSe or a $SnSe_2$ film on a SnSe-$SnSe_2$ eutectic are the large lattice mismatch and the sublimation of the eutectic at a relatively low temperature.

In order that semiconductor eutectics be fabricated as devices, it is necessary that the two constituent phases of the eutectic mixture should have a good lattice match. Thus, it is recommended that eutectic systems with cubic crystal structure be adopted as appropriate materials for device fabrication.

BIBLIOGRAPHY

1. F.S. Galasso, "Unidirectionally Solidified Eutectics for Optical, Electronic and Magnetic Applications", J. of Metals, 6, 17 (1967).

2. F.S. Galasso, F.C. Douglas, and J.A. Batt, "Recent Studies of Eutectics for Nonstructural Applications", J. of Metals, 6, 40 (1970).

3. M.B. Bever, P.E. Duwez, and W.A. Tiller, "On Nonstructural Applications of Composites", Mater. Sci. Eng., 6, 149 (1970).

4. W. Albers, "Physical Properties of Composite Materials", Proc. of the Conf. on In Situ Composites, 1 September (1972).

5. H. Weiss, "Electromagnetic Properties of Eutectic Composites (A Critical Review)", Met. Trans. 2, 1513 (1971).

6. B. Paul and H. Weiss, "Anisotropic InSb-NiSb as an Infrared Detector", Solid State Electronics, 11, 979 (1968).

7. Br. Patent 1,119,215 (1968), "Semiconductor Arrangements for Generating Electromagnetic Radiation in the Range Consisting of the Infrared and Visible Spectral Ranges".

8. A.J. Sievers, "Optical Properties of Composite Structures", Proc. of the Conf. on In Situ Composites, 129, September (1972).

9. B. Reiss and T. Renner, "Der Gerichtete Einbau von Schwemetallphasen in GaAs", Z. Naturforsch. 21A, 546 (1966).

10. A. Muller and M. Wilhelm, "Uber Den Gerichteten Einbau von Schwermetallphasen in $A^{III}B^{V}$ - Verbindungen, Die Eutektika InSb-NiSb, InSb-FeSb, InSb-MnSb und InSb-CrSb", J. Phys. Chem. Solids, 26, 2021 (1965).

11. A. Muller and M. Wilhelm, "Das Eutektikum InSb-Mg_3Sb_2", Z. Naturforsch 21, 555 (1966).

12. A. Muller and M. Wilhelm, "Die Binaren Eutektika GaSb-GaV_3Sb_5 und GaSb-V_2Ga_5", J. Phys. Chem. Solids, 28, 219 (1967).

13. M.I. Karakhanova, A.S. Pashinkin, and A.V. Novoselova, "The Phase Diagram of the Tin-Selenium Systems", Izv. AN SSSR. Neorganish. Materialy. 2 (17), 1186 (1966).

14. A.M. Gas'kov, V.P. Zlomanov, Ju. A. Sapozhnikov, and A.V. Novoselova, Vest. Mosk. Univ. 3, 48 (1968).

15. P.A. Lee and G. Said, "Optical Properties of Tin Diselenide Single Crystals", J. of Phys. D., 1, 837 (1968).

16. W. Albers, C. Haas, H. Ober, G.R. Shodder, and J.D. Wasscher, "Preparation and Properties of Mixed Crystals $SnS_{1-x}Se_x$", J. Phys. Chem. Solids, 23, 215 (1962).

17. W. Albers and J. Verberkt, "The SnSe-$SnSe_2$ Eutectic; a P-N Multilayer Structure", J. of Mat. Science, 5, 24 (1970).

18. W. Albers and J. Verberkt, "The SnSe-$SnSe_2$ Eutectic; a P-N Multilayer Structure", J. of Mat. Sci. 5, 24-28 (1970).

19. L.P. Hunter, (ed), "Handbook of Semiconductor Electronics", 1970, McGraw-Hill Book Company.

20. J.K. Kung and W.G. Spitzer, "Infrared Reflectivity and Free Carrier Absorption of Si-Doped, N-Type GaAs", J. Electrochem. Soc. 121 (11), 1482, November (1974).

21. S. Perkowitz, "Mobility and Infrared Absorption in N-Type Gallium Arsenide", J. of Appl. Phys. 40 (9), 3751, August (1969).

22. P.A. Shumann, Jr., "Plasma Resonance Calibration Curves for Silicon, Germanium, and Gallium Arsenide", Solid State Tech., 50, January (1970).

23. J.R. Dixon and H.R. Riedl, "Electric-Susceptibility Hole Mass of Lead Telluride", Phys. Rev. 138 (3A), A873, May (1965).

24. J.R. Dixon and H.R. Riedl, "Optical Dispersion of Lead Sulphide in the Infrared", Phys. Rev. 140 (4A), A1283, November (1965).

25. D.M. Korn and R. Braunstein, "Infrared Reflectivity Studies of P-type $Pb_{1-x}Sn_xTe$", Phys. Stat. Sol. (b), 50, 77, 1972.

26. E. Mooser and W.B. Pearson, "New Semiconducting Compounds", Phys. Rev. 101, 492 (1956).

27. G. Busch, C. Frohlich, and F. Hullinger, Struktur, Elektrische und Thermoelektrische, "Eigenschafter von $SnSe_2$", Helv. Phys. Acta. 34, 359 (1961).

28. S. Asanabe, "Semiconducting Properties of $SnSe_2$ and $GeSe_2$", J. Phys. Soc. Japan, 16, 1789 (1961).

29. M.T. Kostyshin and P.F. Romanenko, "The Dispersion of Certain Semiconductors in the Neighborhood of Absorption Bands", Opt. Spectrosc. 12, 349 (1962).

30. G. Domingo, R.S. Itoga, and C.R. Kannewurt, "Fundamental Optical Absorption in SnS_2 and $SnSe_2$", Phys. Rev. 143, 536 (1966).

31. P.A. Lee and G. Said, "Optical Properties of Tin Di-Selenide Single Crystals", Brit. J. Appl. Phys. 1, 837 (1968).

32. B.L. Evans and R.A. Hazelwood, "Optical and Electrical Properties of $SnSe_2$", Brit. J. Appl. Phys. 2, 1507 (1969).

33. A.K. Garg, O.P. Agnihotri, and A.K. Jain, "Optical Absorption Spectrum of Tin Diselenide Single Crystals", J. of Appl. Phys. 47 (3), 997 (1976).

34. M.Y. Au-Yang and Marvin L. Cohen, "Electronic Structure and Optical Properties of SnS_2 and $SnSe_2$", Phys. Rev. 178, 1279 (1969).

35. C.Y. Fong and M.L. Cohen, "Electronic Energy-Band Structure of SnS_2 and $SnSe_2$", Phys. Rev. B5, 3095 (1972).

36. R.H. William, R.B. Murray, D.W. Govan, J.M. Thomas, and E.L. Evans, "Band Structure and Photoemission Studies of SnS_2 and $SnSe_2$", J. Phys. C. Solid State Phys. 6, 3631 (1973).

37. D. Chun, R.M. Walser, R.W. Bene and T.H. Coutney, "Polarity-dependent Memory Switching in Devices with SnSe and $SnSe_2$ Crystals", App. Phys. Lett. 24 (10), 479 (1974).

38. N.I. Karakhanova, A.S. Pashinkin, and A.V. Novoselova, "Determining the Dissociation Pressure of Solid Tin Diselenide", Izv. AN SSSR. Neorganish. Materialy. 3 (9), 1550 (1967).

39. R. Colin and J. Drowart, "Thermodynamic Study of Tin Selenide and Tin Telluride Using a Mass Spectrometer", Trans. Farad. Soc. 60, 673 (1964).

40. E.A. Kulykhina, V.P. Zlomanov, and A.V. Novoselova, "P-T Projection of the Phase Diagram of the System SnSe-Se", Izv. AN SSSR. Neorganish. Materialy. 13 (2), 237 (1977).

41. F.H. Nicoll, "The Use of Close Spacing in Chemical-Transport-Systems for Growing Epitaxial Layers of Semiconductors", J. Electrochem. Soc., 110, 1165 (1963).

42. E. Stirl, "Die Sandwich Methode-Ein Neues Verfahren Zur Herstellung Epitaktisch Gewachsener Hulbleiterschichten", J. Phys. Chem. Solids, 24, 1285 (1963).

43. R.F. Tramposch, "Epitaxial Films of Germanium Deposited on Sapphire via Chemical Vapor Transport", J. Electrochem. Soc. 116, 653 (1969).

44. J.E. May, "Kinetics of Epitaxial Silicon Deposition by a Low Pressure Iodide Process", J. Electrochem. Soc., 112, 710 (1965).

45. A.V. Kovda and S.A. Semiletov, Sov. Phys. Crystallorgr. 12, 468 (1967).

46. N.P. Sajin and V.N. Maslov, "Dopl. Akad. Nauk. SSSR, 160, 420(1965).

47. J.F. Nicolau, K.W. Benz, and J.V. Fischback, "InP Epitaxial Growth by the Close-Spaced Method", Proceedings of the 4th International Symposium on GaAs, 11 (1973), (Institute of Phys., New York).

48. A. Yoshikawa and Y. Sakai, "Growth and Properties of CdS Epitaxial Layers by the Close-Spaced Technique", J. of Appl. Phys. 45 (8), 3521 (1974).

49. H.J. Hovel and A.G. Milnes, "The Epitaxy of ZnSe on Ge, GaAs and ZnSe by an HCℓ Close-Spaced-Transport Process", J. Electrochem. Soc. 116, 843 (1969).

50. K. Mitchell, A.L. Fahrenbruch, and R.J. Bube, "Structure and Electrical Properties of CdS and CdTe Thick Film for Solar Cell Application", J. Vac. Sci. Technol. 12, 909 (1975).

51. O.N. Tufte and E.L. Stelzer, "Growth and Properties of $Hg_{1-x}Cd_xTe$ Epitaxial Layers", J. Appl. Phys. 40, 4559 (1969).

52. G. Cohen-Solal and Y. Riant, "Epitaxial (CdHg)Te Infrared Photovoltaic Detectors", Appl. Phys. Lett., 19, 436 (1971).

53. H. Schafer, "Thermodynamische Gesichtspunkte Bei Der Auswahl Chemischer Transportuorgange", J. Cryst. Growth, 9, 17 (1971).

54. R. Nitsche, Fortsch. Miner, 44, 231 (1967).

55. A. Okasaki, "The Crystal Structure of Stannous Selenide SnSe", J. Phys. Soc. Japan, 11, 470 (1956).

56. A. Okasaki, "The Crystal Structure of Germanium Selenide GeSe", J. Phys. Soc. Japan, 13, 1151 (1958).

57. S. Asanabe, "Electrical Properties of Stannous Selenide", J. Phys. Soc. Japan, 14, 281 (1959).

58. J. Umeda, "Electrical Properties of Sb-Doped N-Type SnSe", J. Phys. Soc. Japan, 16, 124 (1961).

59. Y. Mochida, "Optical Properties of Stannous Selenide in the Fundamental Absorption Edge Region", Science of Light, 7 (2), 57 (1968).

60. M. Schieber, "Technology of Crystal Growth", UCLA Extension Course Engineering 881.19, June 17-21, 1974.

61. L.P. Hunter, (ed)., "Handbook of Semiconductor Electronics", Third Edition, McGraw-Hill Book Company.

62. J. Bardeen, F.J. Blatt, and L.H. Hall, "Photoconductivity Conf., Atlantic City, John Wiley & Son, New York (1956), p. 146.

63. A. Bradford and E. Wentworth, "Preparation of Vapor Grown Lead-Tin Telluride for 8-14 Micrometer Photodiodes", Infrared Phys., 15, 303 (1975).

64. A.S. Tenney and M. Ghezzo, "Etch Rates of Doped Oxides in Solutions of Buffered HF", J. Electrochem. Soc., 120 (8), 1091 (1973).

MISSION
of
Rome Air Development Center

RADC plans and executes research, development, test and selected acquisition programs in support of Command, Control Communications and Intelligence (C^3I) activities. Technical and engineering support within areas of technical competence is provided to ESD Program Offices (POs) and other ESD elements. The principal technical mission areas are communications, electromagnetic guidance and control, surveillance of ground and aerospace objects, intelligence data collection and handling, information system technology, solid state sciences, electromagnetics and electronic reliability, maintainability and compatibility.

Printed by
United States Air Force
Hanscom AFB, Mass. 01731

END

5-87

DTIC